



Optimal retrofit strategy using viscous dampers between adjacent RC and SMRFs prone to earthquake-induced pounding

N. Asgarkhani¹ · F. Kazemi¹ · R. Jankowski¹

Received: 9 June 2022 / Revised: 3 September 2022 / Accepted: 1 October 2022
© The Author(s) 2022

Abstract

Nowadays, retrofitting-damaged buildings is an important challenge for engineers. Finding the optimal placement of Viscous Dampers (VDs) between adjacent structures prone to earthquake-induced pounding can help designers to implement VDs with optimizing the cost of construction and achieving higher performance levels for both structures. In this research, the optimal placement of linear and nonlinear VDs between the 3-story, 5-story, and 9-story Steel and RC Moment-Resisting Frames (SMRFs and RC MRFs) is investigated. It is shown that the pounding phenomenon can significantly affect the seismic performance capacities of buildings during earthquakes, and using VDs can improve the seismic limit-state capacities of buildings for retrofitting purposes. For this goal, the seismic limit-state capacities of both colliding structures were assessed using Incremental Dynamic Analysis (IDA) assuming Near-fault Pulse-Like, Near-fault No-Pulse, and Far-Fault seismic records suggested by FEMA-P695. To perform IDAs, structures were modeled according to the seismic codes using a developed algorithm in Matlab and OpenSees software with the ability to remove a collapsed structure during the analysis. The results present an optimal placement for using VDs between structures and also compare the possible conditions to implement VDs. Using these results, engineers can approximately predict the seismic performance levels of both structures prone to earthquake-induced pounding and their final performance after retrofitting. Finally, retrofitting modification factors were proposed to help designers to predict the limit-state performance levels of retrofitted colliding structures without involving complicated and time-consuming analyses.

Keywords Viscous dampers · Structural pounding · Seismic retrofitting · Retrofitting modification factor · Seismic limit-state capacity · Incremental dynamic analysis

1 Introduction

Researchers have investigated the earthquake-induced pounding phenomenon, especially the influence of the impact force as an unexpected additional force for structures [1–4]. The importance of these studies is related to the fact that many buildings were constructed without sufficient in-between Separation Distance (SD) and pounding between

them during earthquakes can impose crucial damages or total destruction. In addition, the design process of structures in the past neglected this external force, as the minimum SD between adjacent structures was not considered in the old seismic codes. Neglecting the SD between the newly constructed buildings also takes place because of the land price in populated cities and lack of a proper monitoring system of construction of buildings [1–3]. There are many examples of such a situation, as it can be seen in Fig. 1.

Although the current seismic codes prescribe a minimum SD, some factors such as an irregular plan or different center of rigidity, which can lead to a torsional movement, make this distance ineffective. Researchers categorized structural pounding as: the floor-to-floor or the floor-to-column pounding [4–8], pounding due to difference in weight of adjacent structures [5, 9, 10], eccentric or non-eccentric pounding [11, 12], and pounding between unequal-height buildings in series [13, 14].

✉ F. Kazemi
farzin.kazemi@pg.edu.pl

N. Asgarkhani
neda.asgarkhani@pg.edu.pl

R. Jankowski
jankowr@pg.edu.pl

¹ Faculty of Civil and Environmental Engineering, Gdańsk University of Technology, ul. Narutowicza 11/12, 80-233 Gdansk, Poland

Fig. 1 Newly constructed adjacent buildings without sufficient SD, and with different base and floors levels (Qazvin, Iran)



The nature of the earthquake-induced pounding phenomenon is a highly-complex engineering problem that should be solved by engineers. Due to this complexity, researchers proposed some ways to control collisions between adjacent structures. One possible solution is to increase the stiffness of the structural members and finally reduce the lateral displacements. Although this approach can be used in all types of structures, this may impose the increase in the construction cost and architectural issues. Therefore, researchers proposed using energy dissipation devices due to their ability to control both displacements and accelerations that are the main features of the pounding phenomenon [15–17]. Raheem [18] conducted the parametric study on the adjacent buildings exposed to earthquakes using linear and nonlinear contact models for different SDs. He proposed to use a shock absorber that reduces the acceleration peaks and finally the impact force. In a more general work, Raheem et al. [19] investigated the effects of eccentric alignment of three, six, and twelve-story adjacent structures under nine earthquakes using a viscoelastic impact model. Their results confirm that the eccentric alignments make the design more complicated and the corners of buildings play a key role against the torsional response of eccentric pounding. Impact-absorbing materials were also considered and a number of studies were carried out using polystyrene bumpers and polymer elements [20–22] and rubber shock absorbers [23, 24]. To overcome the pounding impact, Jankowski and Mahmoud [25] connected the three-story adjacent structures with link elements using spring, dashpots, and viscoelastic elements. The results showed that using viscoelastic elements reduced the peak displacement response of structures compared to dashpot or spring elements applied alone. Regarding this approach, other studies were also carried for viscous dampers (VDs) [26–31], tuned mass dampers [32], friction dampers [33], and multi-link viscoelastic elements [34] installed at the floor levels of buildings where larger probability of

collisions is expected. The Linear or Nonlinear Viscous Dampers (LVDs or NVDs) may have different properties. Martinez-Rodrigo and Romero [35] compared the use of the LVDs and NVDs, and found out that the larger reduction occurred in the case of LVDs while the NVDs achieved smaller damping force. Increasing the number of VDs would not certainly be related to their efficiency [36, 37], while the distribution of VDs had significant effects on structural modal properties [38]. Adding LVDs at all floor levels of the adjacent steel and reinforced concrete structures were proposed by Kazemi et al. [39]. This approach eliminates the sudden changes in impact force, and therefore reduces the possibility of structural damages due to the pounding phenomenon.

The purpose of this study is to investigate an optimal placement of LVDs or NVDs between Steel and RC Moment-Resisting Frames (SMRFs and RC MRFs) prone to earthquake-induced pounding considering the optimized cost of implementation and the seismic limit-state capacity performance level as targets. Therefore, the seismic performance levels of both adjacent structures were investigated, while implementing LVDs or NVDs can affect the seismic behavior of both of them. In addition, based on the results of this study, modification factors for retrofitted structures are determined that can provide a practical tool for estimating proposed retrofitting strategy on the newly constructed or existing structures.

2 Methods of modeling

2.1 Modeling approach of adjacent buildings

To study the pounding phenomenon, the 3-, 5-, and 9-story SMRFs and RC MRFs were considered to be constructed in California with seismic design parameters of $SD_5 = 1.0$ g

and $SD_1 = 0.6$ g and soil type of D (see Fig. 2 for their structural plan). To model the structures, the seismic codes of ASCE 7-16 [40], ANSI/AISC 360-16 [41], ANSI/AISC 341-16 [42], and ACI 318-14 [43] were used. The design coefficients and factors for assumed structures were considered according to the seismic code of ASCE 7-16 [40] (Table 12.2-1), having dead and live loads of 8.379 kN/

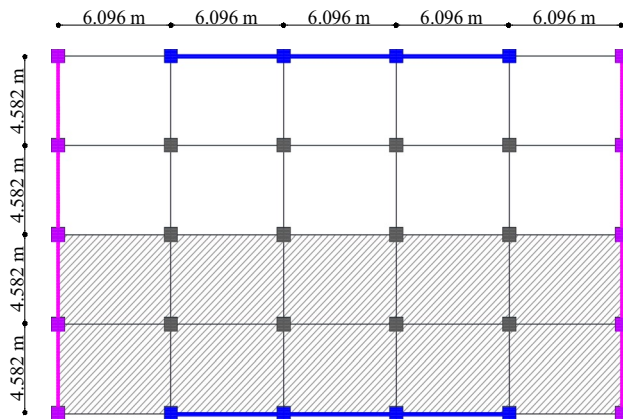
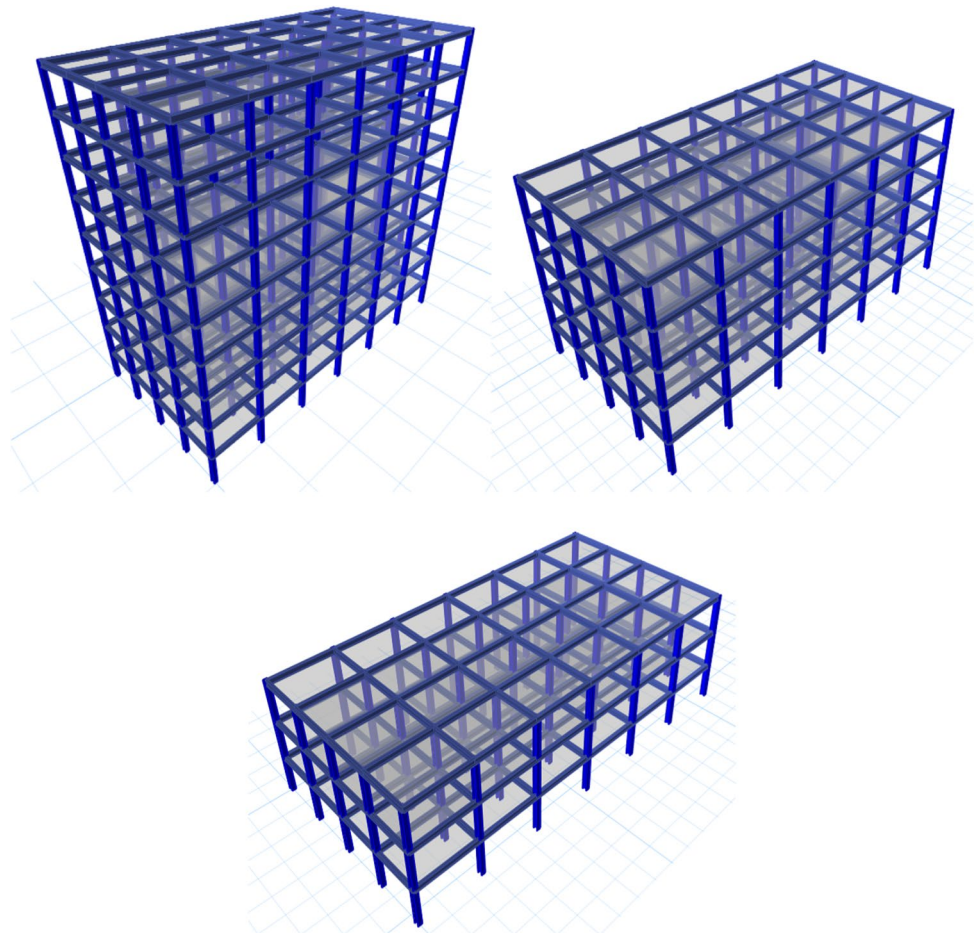


Fig. 2 Considered plan for modeling steel and RC MRFs

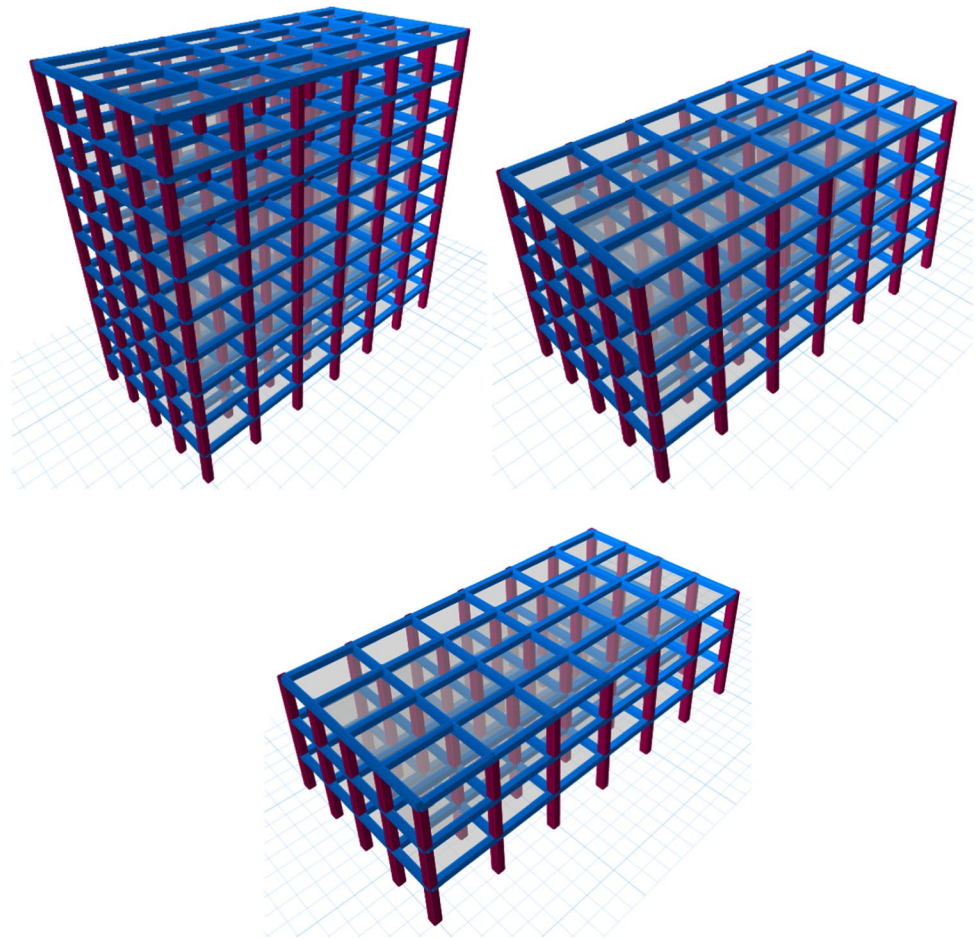
Fig. 3 Three-dimensional view of the 3-, 5-, and 9-story SMRFs



m^2 and 2.39 kN/ m^2 , respectively. Based on the procedures of modeling used by Kitayama and Constantinou [44] and Haselton and Deierlein [45], it is possible to model three-dimensional building by a two-dimensional structure. For this purpose, the main columns of MRFs are used (columns with thick blue lines in Fig. 2 show the MRFs in the X direction), which are connected to the leaning column taking into account the other gravity columns effects. Using the leaning column provides the possibility of considering the P -delta effects with acceptable accuracy of modeling (e.g. see [7, 9, 46]). For modeling structures, the concrete compressive strength of 34.5 MPa, the steel yield strength and Young's modulus of 345 MPa and 200 GPa, respectively, were assumed in the analysis. Figures 3 and 4 show the three-dimensional view of the 3-, 5-, and 9-story SMRFs and RC MRFs, respectively.

For SMRFs, the moment-rotation behavior of the structural elements were defined considering a nonlinear rotational spring at both ends of each member. The behavior of the spring was simulated based on the modified Ibarra–Krawinkler bilinear-hysteretic model (for more detail see [39, 46]) and it was assigned using the zero-length element. The Ibarra–Krawinkler model can

Fig. 4 Three-dimensional view of the 3-, 5-, and 9-story RC MRFs



simulate the cyclic deterioration including unloading and reloading stiffness, strength and post-capping strength. Figure 5 presents the two-dimensional model and the modified Ibarra–Krawinkler model used for defining the nonlinear behavior of elements. It should be noted that 316 specimens were used to calibrate the model with wide range of *W*-sections [39–46]. Therefore, it is possible to

calculate the parameters of hysteresis curves using formula introduced by Lignos and Krawinkler [47].

To model beams and columns of RC MRFs, a trilinear backbone curve of deterioration model, mainly developed by Ibarra et al. [48] and implemented in Opensees [49] software by Altoontash [50], was used. This model can capture the modes of cyclic degradation and collapse states. Two main sources were used for determining the model parameters: the

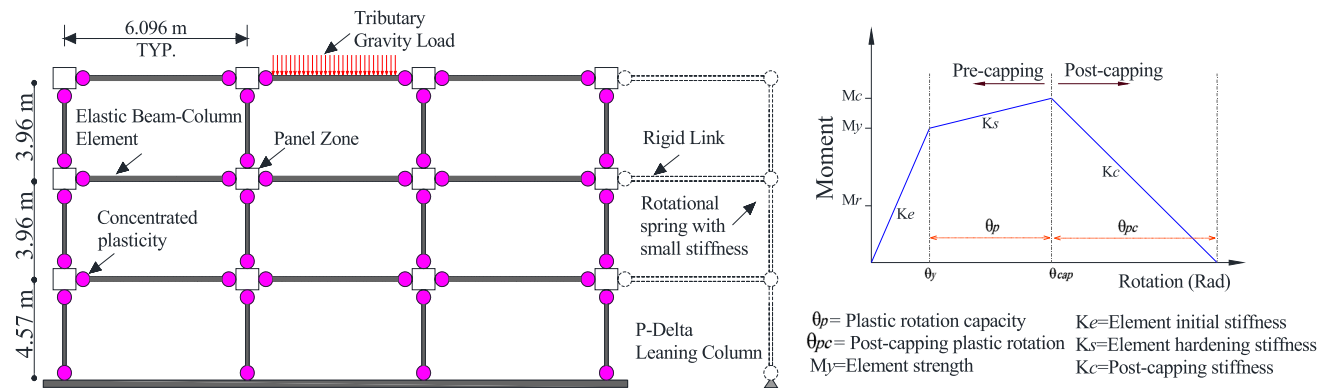


Fig. 5 Two-dimensional model and the modified Ibarra–Krawinkler model used for defining the nonlinear behavior of elements

first one is based on the relationships introduced by Fardis and Biskinis [51], and the second one is based on the experimental specimens of columns investigated by Berry et al. [52]. A number of studies were performed based on this model to capture the seismic collapse capacity of the RC MRFs (e.g. see [39, 53, 54]). Structural documentation of the columns and beams of RC MRFs and SMRFs are presented in Tables 1 and 2.

2.2 Impact contact element

To simulate the structural pounding phenomenon, researchers used different element force models that can precisely model the impact force with high accuracy. The viscoelastic contact element (Kelvin-Voigt element) with high acceptable accuracy was used in this study [54, 55]. The implementation of viscoelastic contact element was validated by Kazemi et al. [5] using the following formula:

$$F(t) = K_{\text{imp}}\delta(t) + C_{\text{imp}}\dot{\delta}(t) \quad (1)$$

$$C_{\text{imp}} = 2\xi\sqrt{K_{\text{imp}}\frac{m_1m_2}{m_1+m_2}} \quad (2)$$

$$\xi = \frac{-\ln(e)}{\sqrt{\pi^2 + (\ln e)^2}} \quad (3)$$

where $F(t)$ is the impact force, C_{imp} and K_{imp} are impact damping and stiffness coefficients, and relative deformation and velocity are expressed as $\delta(t)$ and $\dot{\delta}(t)$. m_1 and m_2 are masses of particular stories of adjacent structures, and ξ is the impact damping ratio [56–58]. The coefficient of restitution, e , was assumed equal to 0.65 (e.g. see [39, 46, 54–59]). According to Polycarpou et al. [12] approach for modeling the three-dimensional adjacent structure, the dimensionless impact stiffness, K_i , in the contact region can be determined as follows:

$$K_i = \left[\frac{1 - \nu_1^2}{E_{\text{Dyn},1}} + \frac{1 - \nu_2^2}{E_{\text{Dyn},2}} \right]^{-1} \quad (4)$$

$$E_{\text{Dyn},i} = 5.82(E_{\text{Static},i})^{0.63} \quad (5)$$

where ν_i and $E_{\text{Dyn},i}$ are the Poisson's ratio and the dynamic elastic modulus of contact material. Considering the $E_{\text{Static}} = 21$ GPa and $\nu_i = 0.2$ are used for normal strength concrete, the dimensionless impact stiffness, K_i , can be calculated from Eqs. 4 and 5 as equal to $K_i = 209.6 \times 10^5$ kN/m². Moreover, assuming the half of structural plan (see Fig. 2) in pounding condition (9.144 m), the impact damping and

Table 1 Structural documentation of the columns of RC MRFs

Model	Story	Exterior					Interior				
		h (cm)	b (cm)	s^* (cm)	ρ_{tot}^{**}	ρ_{sh}^{***}	h (cm)	b (cm)	s (cm)	ρ_{tot}	ρ_{sh}
3-Story RC MRF	1st	76.2	71.1	12.7	0.0135	0.01	76.2	71.1	12.7	0.017	0.01
	2nd	76.2	71.1	12.7	0.01	0.01	76.2	71.1	12.7	0.017	0.01
	3rd	76.2	71.1	12.7	0.01	0.01	76.2	71.1	12.7	0.017	0.01
5-Story RC MRF	1st	76.2	81.3	8.9	0.02	0.0085	96.5	81.3	8.9	0.016	0.0112
	2nd	76.2	81.3	8.9	0.02	0.0085	96.5	81.3	8.9	0.016	0.008
	3rd	76.2	81.3	10.2	0.01	0.006	96.5	81.3	8.9	0.01	0.008
	4th	76.2	81.3	10.2	0.01	0.006	96.5	81.3	8.9	0.01	0.008
	5th	76.2	81.3	10.2	0.01	0.006	96.5	81.3	8.9	0.01	0.008
9-Story RC MRF	1st	71.1	66.05	8.9	0.02	0.01	86.4	66.05	8.9	0.018	0.012
	2nd	71.1	66.05	8.9	0.015	0.01	86.4	66.05	8.9	0.013	0.012
	3rd	71.1	66.05	8.9	0.015	0.01	86.4	66.05	8.9	0.013	0.012
	4th	71.1	66.05	10.2	0.015	0.01	86.4	66.05	8.9	0.013	0.012
	5th	71.1	66.05	10.2	0.015	0.007	86.4	66.05	8.9	0.022	0.007
	6th	71.1	66.05	10.2	0.01	0.007	71.1	66.05	10.2	0.015	0.007
	7th	71.1	66.05	10.2	0.01	0.007	71.1	66.05	10.2	0.014	0.007
	8th	71.1	66.05	10.2	0.01	0.007	71.1	66.05	10.2	0.01	0.007
	9th	71.1	66.05	10.2	0.01	0.007	71.1	66.05	10.2	0.01	0.007

* s spacing of transverse reinforcement

** ρ_{tot} ratio of total longitudinal reinforcement area

*** ρ_{sh} ratio of transverse reinforcement area

Table 2 Structural documentation of SMRFs and RC MRFs

Model	Story	RC MRF						SMRF		
		Exterior and interior beam						Interior column	Exterior column	Beam
		h (cm)	b (cm)	s (cm)	ρ	ρ'^*	ρ_{sh}			
3-Story	1st	71.1	71.1	12.7	0.0065	0.0075	0.004	W14X176	W14X176	W24X68
	2nd	71.1	71.1	12.7	0.0065	0.0075	0.004	W14X176	W14X176	W21X55
	3rd	71.1	71.1	12.7	0.0065	0.0075	0.004	W14X145	W14X145	W18X40
5-Story	1st	61	81.3	12.7	0.0108	0.012	0.005	W14X211	W14X211	W24X68
	2nd	61	81.3	12.7	0.01	0.0115	0.005	W14X211	W14X211	W24X68
	3rd	61	81.3	12.7	0.009	0.018	0.004	W14X211	W14X211	W24X68
	4th	61	81.3	12.7	0.005	0.006	0.003	W14X176	W14X176	W21X50
	5th	61	81.3	12.7	0.005	0.006	0.003	W14X176	W14X176	W18X40
9-Story	1st	76.2	66.05	12.7	0.007	0.0075	0.004	W14X283	W14X283	W27X84
	2nd	76.2	66.05	16.5	0.007	0.0085	0.0045	W14X283	W14X283	W27X84
	3rd	76.2	66.05	12.7	0.007	0.008	0.004	W14X233	W14X233	W24X76
	4th	76.2	66.05	14	0.006	0.0075	0.004	W14X233	W14X233	W24X76
	5th	76.2	66.05	15.25	0.0055	0.007	0.0037	W14X193	W14X193	W24X68
	6th	76.2	66.05	16.5	0.005	0.005	0.003	W14X193	W14X193	W24X68
	7th	76.2	66.05	14	0.003	0.004	0.0025	W14X159	W14X159	W21X55
	8th	76.2	66.05	15.25	0.003	0.003	0.0025	W14X159	W14X159	W21X55
	9th	76.2	66.05	15.25	0.003	0.003	0.0025	W14X159	W14X159	W18X40

* ρ' ratio of longitudinal reinforcement in compression

stiffness coefficients, C_{imp} and K_{imp} , can be obtained from the equations equal to $C_k = 7576$ kNs/m and $K_{imp} = 19.17 \times 10^7$ kN/m, respectively.

2.3 Models of pounding

Modeling pounding is a very complicated process, including factors such as the local deformation effects, the yielding area, the material of impact area and ductility effects. Although these factors can complicate the modeling process, it has been seen that different damping coefficients and impact stiffness do not significantly affect the results [60]. Hence, the determined values can be approximately considered as appropriate values for the analysis.

To consider the allowable SD, the approach proposed by ASCE 7-16 [40] was used. The adjacent buildings should be separated by the allowable SD, which can be calculated as follows:

$$SD = \sqrt{\left(\frac{C_d \cdot \delta_M}{I}\right)_1^2 + \left(\frac{C_d \cdot \delta_M}{I}\right)_2^2} \quad (6)$$

where δ_M is the maximum inelastic response displacement and C_d and I are the deflection amplification factor and the importance factor, respectively. δ_M for both RC MRFs and SMRFs can be calculated from the nonlinear static analysis (i.e. pushover) having the lateral load distribution of the

first mode shape. This value is used as $1.0D$ between adjacent structures and two other values of 0.0 and $0.5D$ can be assumed. Table 3 presents the considered SDs between RC MRFs and SMRFs.

Table 3 SDs between adjacent RC MRFs and SMRFs

Models	0.0 (cm)	0.5D (cm)	1.0D (cm)
3-Story RC MRFs and 3-story SMRFs	0.0	8.3	16.6
3-Story RC MRFs and 5-story SMRFs	0.0	7.7	15.5
3-Story RC MRFs and 9-story SMRFs	0.0	7.4	14.7
5-Story RC MRFs and 3-story SMRFs	0.0	8.8	17.6
5-Story RC MRFs and 5-story SMRFs	0.0	12.9	25.9
5-Story RC MRFs and 9-story SMRFs	0.0	13.8	27.5
9-Story RC MRFs and 3-story SMRFs	0.0	8.3	16.6
9-Story RC MRFs and 5-story SMRFs	0.0	12.5	25.0
9-Story RC MRFs and 9-story SMRFs	0.0	21.6	43.1

2.4 Using VDs between structures

VD is a kind of energy dissipation device that transforms kinetic energy into heat energy to dissipate the seismic energy due to earthquakes. Equation (7) shows the relation between the VD force, F_{VD} , the damping coefficient, $C(\alpha)$, the relative velocity, \dot{x} , the signum function, sgn , and the damper velocity exponent, α [26–39].

$$F_{FVD} = C(\alpha)|\dot{x}|^\alpha \text{sgn}(\dot{x}) \quad (7)$$

The damper velocity exponent can take values from 0.0 to 1.0 for NVDs or LVDs, respectively. To calculate the supplemental damping ratio, ξ_{VD} , of VDs implemented between adjacent RC MRFs and SMRFs, modified equation introduced by Kandemir-Mazanoglu and Mazanoglu [30] was used:

$$\xi_{VD} = \frac{(\max\{T_{1,1}, T_{1,2}\}) \sum_j C(\alpha)_j (\phi_{j,1} - \phi_{j,2})^2}{4\pi \sum_i m_i \phi_i^2} \quad (8)$$

$$C(\alpha) = \frac{C(\alpha = 1)(\min\{\omega_{1,1}, \omega_{1,2}\}X_0)^{1-\alpha}}{\beta} \quad (9)$$

$$\beta = \frac{2^{2+\alpha}\Gamma^2\left(1 + \frac{\alpha}{2}\right)}{\pi\Gamma(2 + \alpha)} \quad (10)$$

where $T_{1,1}$, $T_{1,2}$ are the fundamental period for the structures, the relative horizontal deformation corresponding to the first mode shape between floor levels of adjacent RC MRFs and SMRFs is obtained by $(\phi_{j,1} - \phi_{j,2})$. Moreover, X_0 is the maximum relative displacement of the adjacent structures, $\omega_{1,1}$ and $\omega_{1,2}$ are the natural frequencies of the adjacent buildings, and Γ is the gamma function. To model VDs, it was considered that the VDs with rigid supporting do not reach their stroke limits during seismic excitations due to assumption of their large enough stroke limits.

In this research, both of NVDs or LVDs were considered between the aforementioned adjacent structures. Assuming three SDs, three ground motion data sets of Near-fault Pulse-Like (NPL), Near-fault No-Pulse (NNP), and Far-Fault (FF) seismic records suggested by FEMA-P695 [61] were used to find out the effects of earthquake events. Table 4 presents all the considered conditions (1086 models). In addition, all structures were analyzed in alone condition.

3 Results of analysis

3.1 Moment-rotation curve

Modified Ibarra–Krawinkler bilinear-hysteretic model (see [62–64]) was used to model the plastic hinges of structural elements. To compare the effects of pounding and implementing LVDs between the structures, the moment-rotation curves were used. Figures 6 and 7 present a comparison between beam and column hinges of the 3-story SMRF colliding with 5-story RC MRF in pounding situation and implementing LVDs between structures, respectively, subjected to NNP record (Northridge, 1/17/1994, Sepulveda VA Hospital station) assuming SD equal to 0.0 and $S_a(T_1) = 0.92$ g. According to results, pounding can increase the maximum rotation of beam and column by 16% and 29.1% (for the beam from 0.042 to 0.050 rad, and for the column from 0.034 to 0.048 rad), respectively. In a structure, columns play a crucial role in the total collapse and the results show that 29.1% of column rotation will be added due to collisions. So it is important to find a solution to resist this sudden force. According to this result, adding VDs between the colliding structures is an alternative. The results confirm that using LVDs between structures can decrease the maximum values of the moment-rotation curves for beams and columns by 48% and 31.25% (for the beam from 0.050 to 0.026 rad, and the column from 0.048 to 0.033 rad), respectively. It is worth mentioning that this reduction can cause overall improvement in performance levels. Similar results were also observed for beams and column hinges of other colliding structures with different SDs and VDs.

3.2 IDA curves of pounding structures

To better investigate the effects of adding VDs on the seismic limit-state capacity of the colliding structures, the Incremental Dynamic Analysis (IDA) was used. Although many intensity measures were introduced by the researchers, $S_a(T_1)$ was selected for this purpose, and IDAs were performed assuming three ground motion sets of NPL, NNP, and FF suggested by FEMA-P695 [61]. OpenSees [49] software is an open-source developed program that can be used for accomplishing computational simulations in earthquake engineering to obtain the structural performances. The structural elements can be defined in interpreter (e.g. Python or Tcl) and different types of numerical solutions can be used for seismic analysis, which includes nonlinear time-history analysis or IDAs. It should be noted that new materials and structural elements have been added in this software to determine seismic behavior

Table 4 Considered adjacent pounding RC MRFs and SMRFs for optimal placement of NVDs or LVDs

Structure 1	Structure 2	Seismic ground motion (FEMA-P695)	SD	Linear or nonlinear VD	Implementation stories	Model name
3-Story SMRF	3-Story RC MRF	NPL	0.0	Alpha 0.3*	2	3St-3RC-1
		NNP	0.5D	Alpha 0.7	3	3St-3RC-2
		FF	1.0D	Alpha 1.0	1, 3	3St-3RC-3
3-Story SMRF	5-Story RC MRF	NPL	0.0	Alpha 0.3	1, 2, 3	3St-3RC-4
					2	3St-5RC-1
					3	3St-5RC-2
					1, 3	3St-5RC-3
3-Story SMRF	9-Story RC MRF	NPL	0.0	Alpha 0.3	1, 2, 3	3St-5RC-4
					2	3St-9RC-1
					3	3St-9RC-2
					1, 3	3St-9RC-3
5-Story SMRF	3-Story RC MRF	NPL	0.0	Alpha 0.3	1, 2, 3	3St-9RC-4
					2	5St-3RC-1
					3	5St-3RC-2
					1, 3	5St-3RC-3
5-Story SMRF	5-Story RC MRF	NPL	0.0	Alpha 0.3	1, 2, 3	5St-3RC-4
					5	5St-5RC-1
					2, 5	5St-5RC-2
					1, 3, 5	5St-5RC-3
5-Story SMRF	9-Story RC MRF	NPL	0.0	Alpha 0.3	1, 2, 3, 4, 5	5St-5RC-4
					5	5St-9RC-1
					2, 5	5St-9RC-2
					1, 3, 5	5St-9RC-3
9-Story SMRF	3-Story RC MRF	NPL	0.0	Alpha 0.3	1, 2, 3, 4, 5	5St-9RC-4
					2	9St-3RC-1
					3	9St-3RC-2
					1, 3	9St-3RC-3
9-Story SMRF	5-Story RC MRF	NPL	0.0	Alpha 0.3	1, 2, 3	9St-3RC-4
					5	9St-5RC-1
					2, 5	9St-5RC-2
					1, 3, 5	9St-5RC-3
9-Story SMRF	9-Story RC MRF	NPL	0.0	Alpha 0.3	1, 2, 3, 4, 5	9St-5RC-4
					9	9St-9RC-1
					5	9St-9RC-2
					9, 5	9St-9RC-3
9-Story SMRF	9-Story RC MRF	NPL	0.0	Alpha 0.3	9, 5, 1	9St-9RC-4
					9, 6, 3	9St-9RC-5
					8, 6, 4, 2	9St-9RC-6
					9, 7, 5, 3, 1	9St-9RC-7
					9, 8, 7, 6, 5, 4, 3, 2, 1	9St-9RC-8

*Alpha presents the damper velocity exponent

of members. To control, monitor and classify the output results, MATLAB [65] was used, which is a programming platform with wide range of capabilities. In real condition, it is possible that RC MRF and SMRF are constructed next to each other. Taking into account the pounding phenomenon, the adjacent structures may have different collapse

states, in which, one of the structures may experience total failure before the next one. Therefore, it is important to consider the real condition of two colliding structures and take into account that one of the structures would collapse before the other one. To tackle this issue, the Tcl programming code, that uses MATLAB [65] and OpenSees [49]

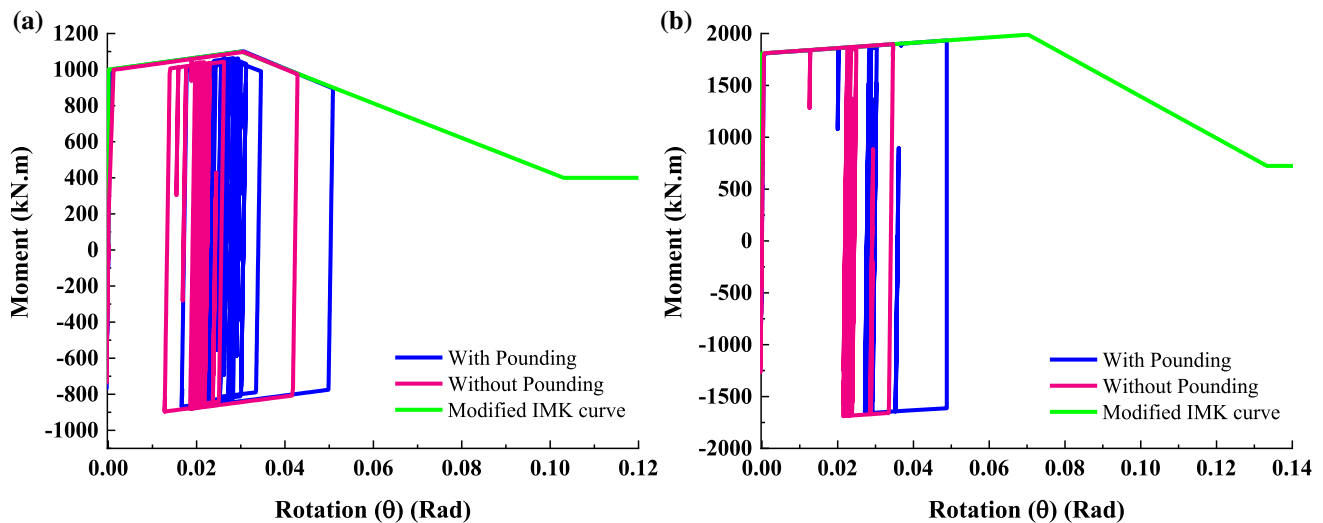


Fig. 6 Comparison between hinges of **a** beam, **b** column of 3rd floor of the 3-story SMRF colliding with 5-story RC MRF assuming SD of 0.0

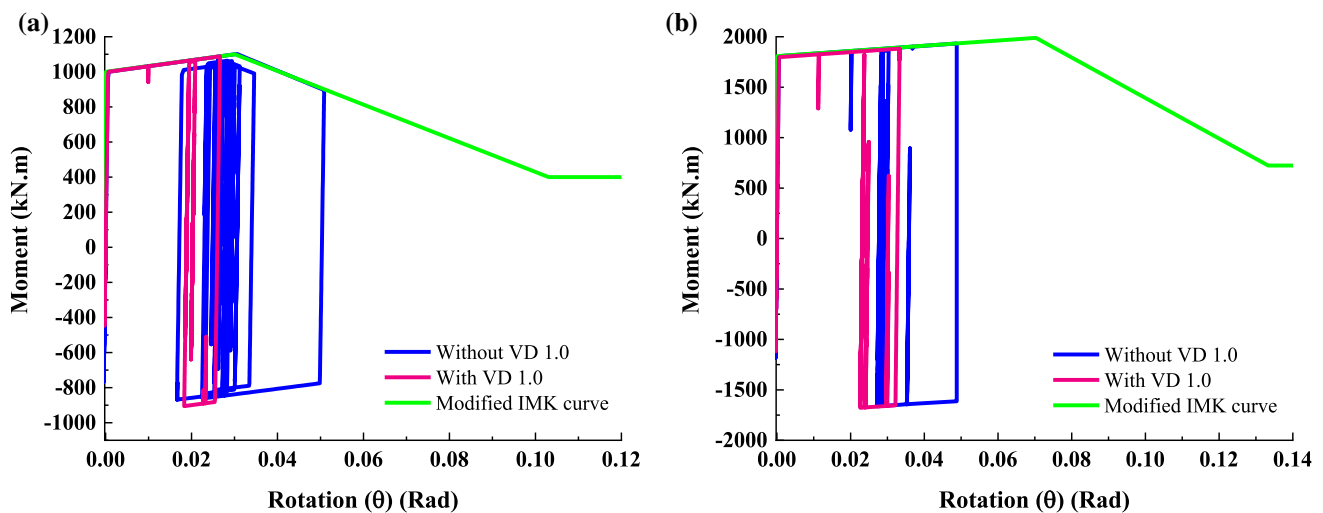


Fig. 7 Comparison between hinges of **a** beam, **b** column of 3rd floor of the 3-story SMRF colliding with 5-story RC MRF considering LVDs in all floor levels for SD of 0.0

softwares simultaneously, was developed. This program allowed us to consider the effects of collapsed structure during the analysis, and this structure was not removed during further analysis until the total collapse of the second structure. In this way, the real condition of pounding phenomenon could be simulated. Using the program, both limit-state capacities of colliding structures can be obtained in one model that decreases the analysis time, and the effects of collapsed structure can be considered in the response of the second structure that can increase the accuracy of modeling. Figure 8 presents the IDA curves (black lines) and the median IDA curves (pink lines)

(M-IDAs) of the 9-story RC MRFs (a) and the 9-story SMRFs (b) subjected to NPL records for SD of 1.0.

3.3 Performance level of structures

Following recommendations of FEMA 356 [66], the allowable interstory drift for primary structural elements were assumed for performance levels of Immediate Occupancy (IO), Life Safety (LS), Collapse Prevention (CP), and total Collapse (C) according to defined damages.

The allowable values of interstory drift ratio of 1.0%, 2.0%, and 4.0%, were assumed for the performance of IO,

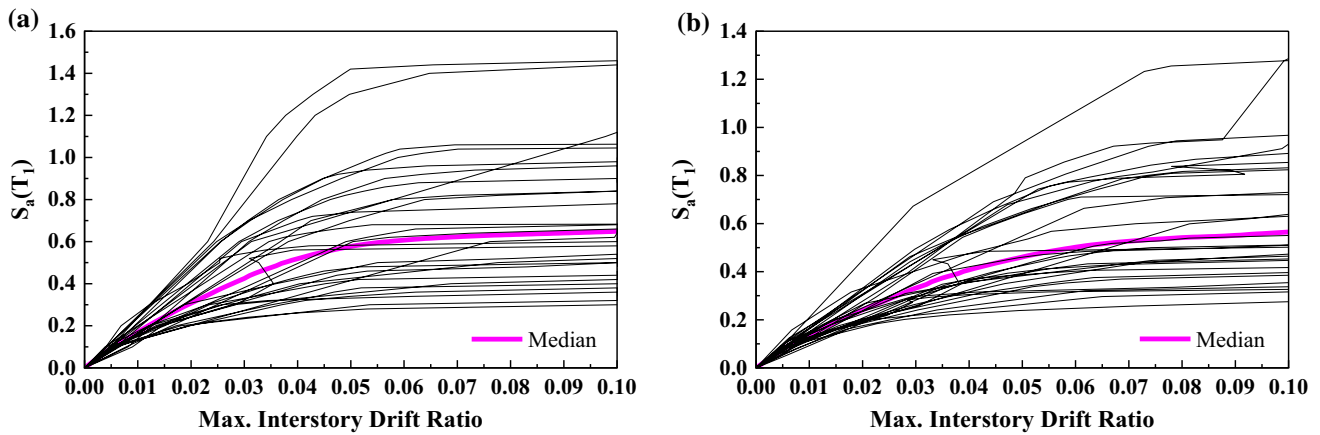


Fig. 8 IDA curves for, **a** the 9-story RC MRFs, **b** the 9-story SMRFs assuming LVDs between all stories subjected to NPL records for SD of 1.0

LS, and CP for RC MRFs, respectively. In addition, for SMRFs, the allowable values of interstory drift ratio of 0.7%, 2.5%, and 5.0%, respectively, were considered. In both structures, the flat part of M-IDAs presents the total collapse of the structure (C). Table 5 shows the performance levels of RC MRFs and SMRFs in no pounding condition considering three record subsets. It can be seen that, in the case of RC MRFs, the values of M-IDAs for assumed performance levels in NNP subset are higher than for other subsets. It is also correct for the 3-story SMRF, while for in the 5-, and 9-story SMRFs, the assumed performance levels in FF subset are higher than for other subsets.

3.4 Comparing implementing NVDs or LVDs

Figure 9 compares the results of using NVDs or LVDs in the floor levels of all stories on M-IDAs of the 3-story SMRF colliding with 3-story RC MRF subjected to NPL for SD of 1.0D. According to Fig. 9, using LVDs between structures prone to pounding can increase M-IDAs of the RC MRFs by 33.06% (from 1.104 to 1.469), while decreasing M-IDAs of the SMRFs by 16.22% (from 1.892 to 1.585). The results confirm that using NVDs or LVDs has the same effect in M-IDAs that increases M-IDAs of RC MRFs and

decreases M-IDAs of SMRFs. In other words, there is no difference between using NVDs or LVDs. These VDs can decrease M-IDAs of 3-story SMRF while increasing M-IDAs of 3-story RC MRF. The amount of M-IDAs in the aforementioned performance levels obtained from the analysis is presented in Table 6. According to this table, in each performance level, M-IDAs can show which kind of VDs have better performance. It can be seen that the LVDs added to all story levels have better performance levels, as compared to the NVDs.

Figure 10 compares the results of using NVDs or LVD in the second-floor level on M-IDAs of the 3-story SMRF colliding with 3-story RC MRF subjected to NPL for SD of 1.0D. It can be seen that the LVD added at the second-floor level increases M-IDAs of the 3-story RC MRF more than NVDs. In addition, LVD added at the second-floor level of the 3-story SMRF causes less reduction in M-IDAs, as compared to NVDs. LVD can also prevent further damages. To better compare the results, Table 7 presents the values of the performance levels of colliding structures in detail. It can be seen from the table that using LVD at the second level of colliding structures results in better performance levels increasing M-IDAs of the 3-story RC MRF by 15.67% (from 1.104 to 1.277) or decreasing M-IDAs of the 3-story

Table 5 Limited state capacities of the RC MRFs and SMRFs in alone condition assuming three record subsets

Subset	3-Story RC				5-Story RC				9-Story RC			
	IO	LS	CP	C	IO	LS	CP	C	IO	LS	CP	C
NPL	0.330	0.556	0.844	1.104	0.264	0.460	0.734	0.988	0.163	0.290	0.450	0.530
NNP	0.395	0.721	1.153	1.539	0.280	0.518	0.853	1.167	0.165	0.302	0.476	0.545
FF	0.375	0.673	1.082	1.338	0.265	0.492	0.850	1.102	0.174	0.318	0.483	0.552
	3-Story steel				5-Story steel				9-Story steel			
NPL	0.226	0.807	1.374	1.893	0.153	0.502	0.946	1.270	0.080	0.274	0.460	0.548
NNP	0.226	0.805	1.454	2.221	0.135	0.481	0.945	1.304	0.061	0.241	0.382	0.465
FF	0.223	0.795	1.454	2.085	0.142	0.546	1.075	1.409	0.065	0.243	0.415	0.513

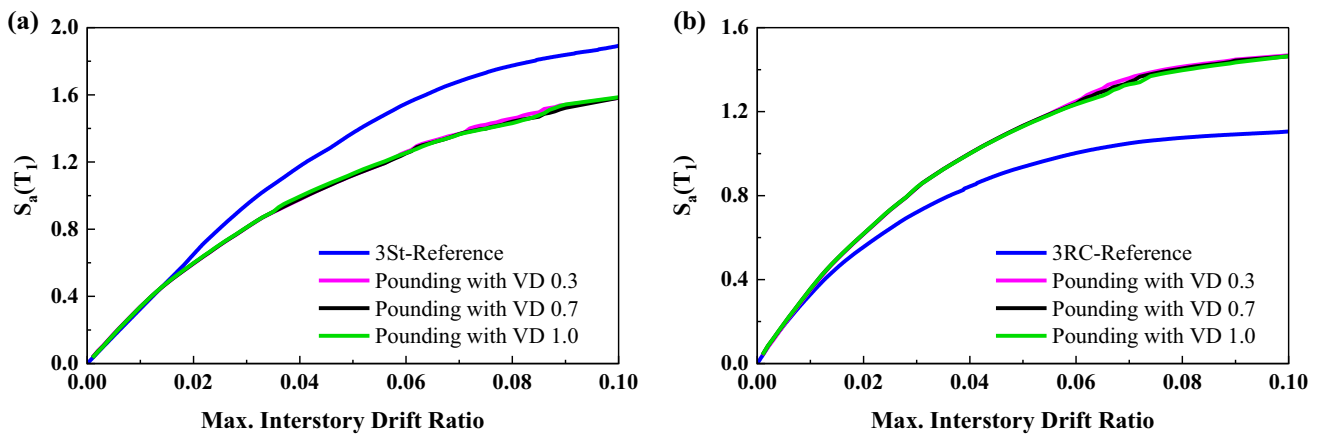


Fig. 9 Comparing the effects of the NVDs or LVDs implemented in all story levels on M-IDAs of **a** the 3-story SMRF, **b** the 3-story RC MRF including NPL record subset for SD of 1.0D

Table 6 Limited state capacities of the 3-story SMRF and the 3-story RC MRF structures with different VDs implemented in all story levels subjected to NPL record subsets for SD of 1.0D

Model name	3-Story SMRF				3-Story RC MRF			
	IO	LS	CP	C	IO	LS	CP	C
3St-3RC-SD1.0D	0.229	0.806	1.373	1.892	0.329	0.555	0.843	1.104
3St-3RC-4-VD 0.3-SD1.0D	0.243	0.705	1.120	1.581	0.350	0.616	1.00	1.468
3St-3RC-4-VD 0.7-SD 1.0D	0.241	0.707	1.121	1.582	0.355	0.618	1.00	1.463
3St-3RC-4-VD 1.0-SD1.0D	0.245	0.709	1.131	1.585	0.357	0.619	1.01	1.469

Bold values indicate the best results obtained from implementing VDs

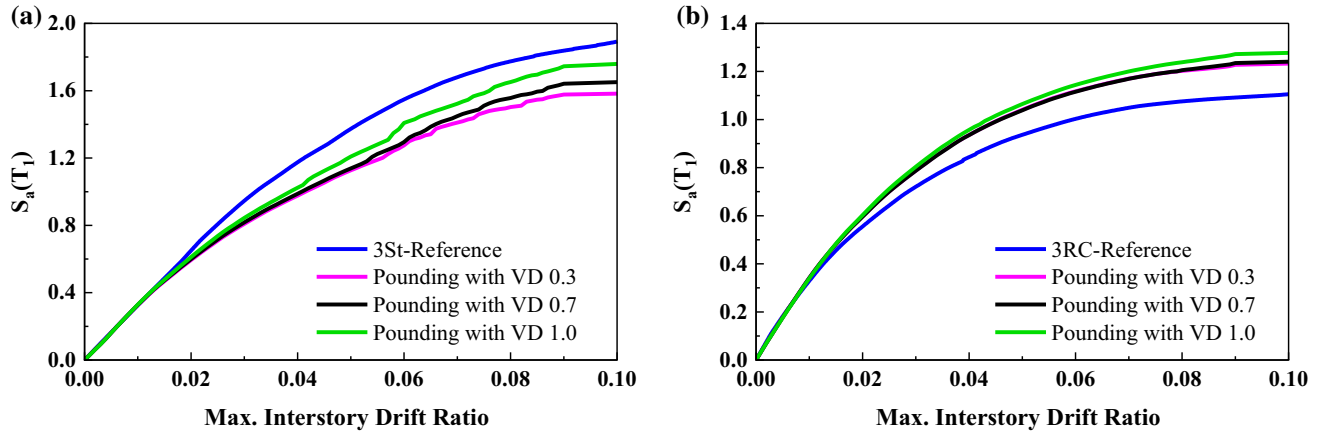


Fig. 10 Comparing the effects of the NVDs or LVDs implemented in 2nd story level on M-IDAs of **a** the 3-story SMRF, **b** the 3-story RC MRF including NPL record subset for SD of 1.0D

Table 7 Limited state capacities of the 3-story SMRF and the 3-story RC MRF assuming different VDs implemented in 2nd story level subjected to NPL record subsets for SD of 1.0D

Model name	3-Story SMRF				3-Story RC MRF			
	IO	LS	CP	C	IO	LS	CP	C
3St-3RC-SD1.0D	0.229	0.806	1.373	1.892	0.329	0.555	0.843	1.104
3St-3RC-1-VD 0.3-SD1.0D	0.229	0.708	1.127	1.582	0.341	0.597	0.936	1.232
3St-3RC-1-VD 0.7-SD1.0D	0.229	0.716	1.138	1.651	0.341	0.596	0.935	1.240
3St-3RC-1-VD 1.0-SD1.0D	0.229	0.736	1.208	1.759	0.341	0.602	0.957	1.277

Bold values indicate the best results obtained from implementing VDs

SMRF by 7.02% (from 1.892 to 1.759). Therefore, according to this sensitivity analysis, the placement of LVDs between adjacent structures will be investigated due to their better performance, as compared to NVDs. It is worth noting that similar results were also observed for other record subsets.

3.5 Comparing M-IDAs of 3-story SMRF pounding with RC MRFs

Figure 11 presents the effects of using LVDs on M-IDAs of the 3-story SMRF and 3-story RC MRF subjected to NPL for SD of 1.0D. The models were defined according to Table 4. Using LVDs at all floor levels (3St-3RC-4) increases M-IDAs for the 3-story RC MRF by 32.48% (from 1.105 to 1.464) which is more than other assumed models considering LVD at the second-floor level (3St-3RC-1), at the third-floor level (3St-3RC-2), and at both first and third-floor level simultaneously (3St-3RC-3) by 12.4%, 13.4%, and 7.3%, respectively. Therefore, the best model to improve the performance levels of the 3-story RC MRF is implementing the LVDs according to the condition defined for 3St-3RC-4 in Table 4. The values of the four performance levels are presented in Table 8. On other side, for improving the performance levels of IO and LS for the 3-story SMRF,

using the condition of 3St-3RC-2, and for the performance levels of CP and C, using the condition of 3St-3RC-3 can be a good alternative. Because these conditions, 3St-3RC-2 and 3St-3RC-3, can cause less reduction in M-IDAs, as compared to other models. Although using the 3St-3RC-4 is the best alternative for the 3-story RC MRF, this condition can cause the largest reduction in M-IDAs of the 3-story SMRF. Therefore, it is suggested to consider both structures' performance levels in retrofitting approach and choose the best model according to required performance levels.

Figure 12 presents the results of using LVDs on M-IDAs of the 3-story SMRF and 5-story RC MRF subjected to NPL for SD of 1.0D. Using LVD at the third-floor level (3St-5RC-2) increases M-IDAs for the 5-story RC MRF by 26.8% (from 0.987 to 1.252) which is more than other assumed models considering LVD at second-floor level (3St-5RC-1), at both first and third-floor level simultaneously (3St-5RC-3), and at all floor levels (3St-5RC-4) by 5.4%, 13.8%, and 12.4%, respectively. Therefore, the best model to improve the performance levels of the 5-story RC MRF is implementing the LVD according to the condition defined for 3St-3RC-2 in Table 4. In addition, for other performance levels, the values are presented in Table 9. For the 3-story SMRF, the 3St-5RC-1 condition is a better alternative in

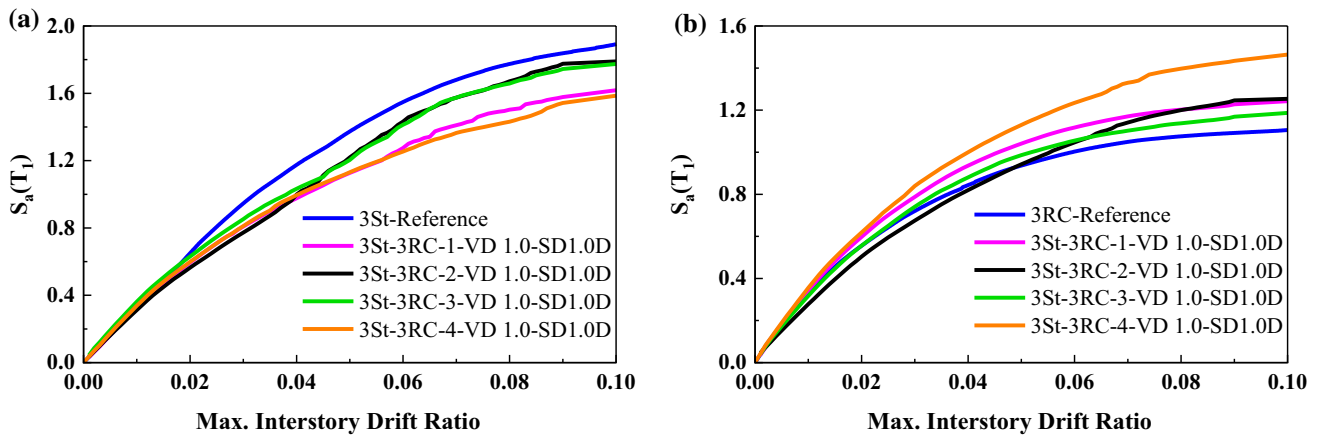


Fig. 11 Comparison M-IDAs of a the 3-story SMRF, b the 3-story RC MRF in pounding condition including NPL record subset for SD of 1.0D

Table 8 Limited state capacities of the 3-story SMRF and the 3-story RC MRF structures subjected to NPL record subsets for SD of 1.0D

Model name	3-Story SMRF				3-Story RC MRF			
	IO	LS	CP	C	IO	LS	CP	C
3St-3RC-SD1.0D	0.229	0.806	1.373	1.892	0.329	0.555	0.843	1.105
3St-3RC-1-VD 1.0-SD1.0D	0.229	0.708	1.127	1.618	0.341	0.597	0.936	1.242
3St-3RC-2-VD 1.0-SD1.0D	0.222	0.670	1.219	1.789	0.277	0.504	0.819	1.253
3St-3RC-3-VD 1.0-SD1.0D	0.261	0.747	1.203	1.774	0.317	0.555	0.880	1.186
3St-3RC-4-VD 1.0-SD1.0D	0.241	0.709	1.131	1.585	0.355	0.618	0.999	1.464

Bold values indicate the best results obtained from implementing VDs

performance levels of IO and LS with improvements in M-IDAs values by 17% and 4.8%, respectively, while this can cause smaller reduction in the performance level of CP by 13.32%. For the performance level of C, the results confirm that the 3St-5RC-3 condition, with the reduction by 4.75%, is the best alternative among all models. Adding LVDs between the structures can cause an increase or

decrease due to the assumed performance levels and the kind of implementation.

Figure 13 presents the results of using LVDs on M-IDAs of the 3-story SMRF and the 9-story RC MRF subjected to NPL for SD of 1.0D. Using LVDs at all floor levels (3St-9RC-4) increases M-IDAs for the 9-story RC MRF in performance levels of IO, LS, and CP by 5.5%, 2.1%, and 12.7%,

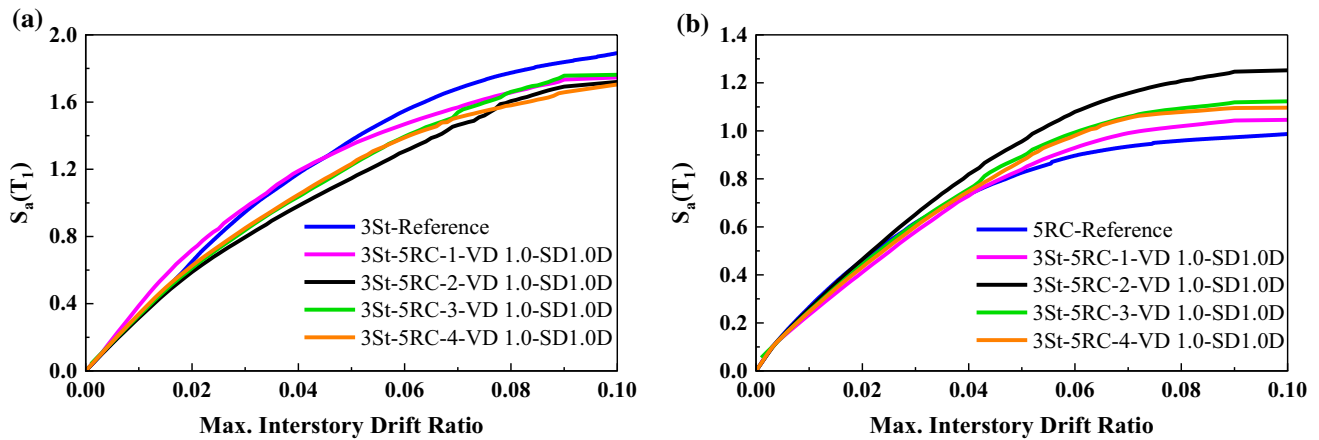


Fig. 12 Comparison M-IDAs of a 3-story SMRF, b 5-story RC MRF in pounding condition including NPL record subset for SD of 1.0D

Table 9 Limited state capacities of the 3-story SMRF and 5-story RC MRF structures subjected to NPL record subsets for SD of 1.0D

Model name	3-Story SMRF				5-Story RC MRF			
	IO	LS	CP	C	IO	LS	CP	C
3St-5RC-SD1.0D	0.229	0.806	1.373	1.892	0.265	0.461	0.734	0.987
3St-5RC-1-VD 1.0-SD1.0D	0.268	0.845	1.190	1.746	0.234	0.411	0.729	1.040
3St-5RC-2-VD 1.0-SD1.0D	0.225	0.697	0.981	1.699	0.258	0.464	0.818	1.252
3St-5RC-3-VD 1.0-SD1.0D	0.230	0.728	1.036	1.802	0.248	0.443	0.756	1.123
3St-5RC-4-VD 1.0-SD1.0D	0.240	0.740	1.048	1.664	0.246	0.432	0.747	1.109

Bold values indicate the best results obtained from implementing VDs

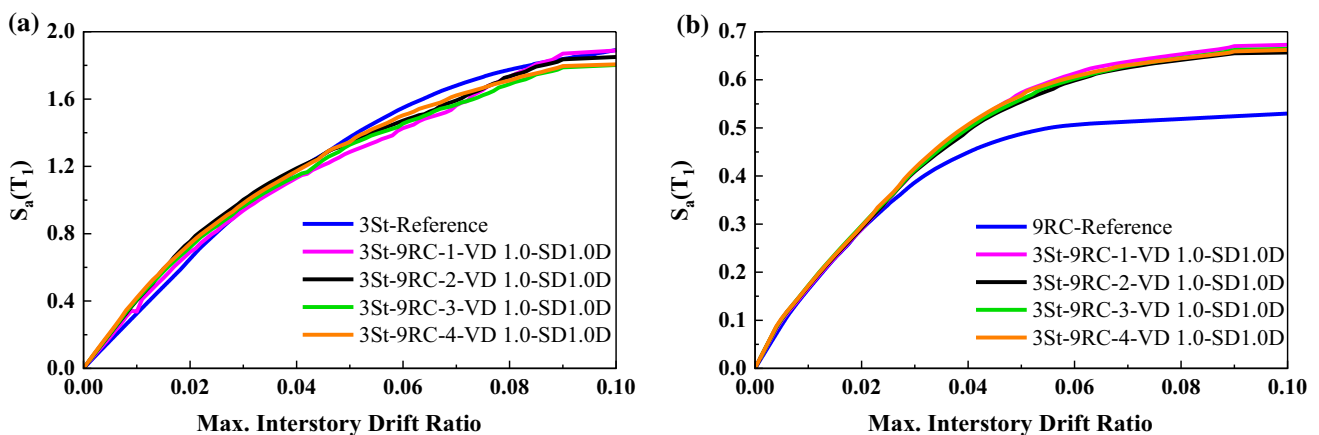


Fig. 13 Comparison M-IDAs of a the 3-story SMRF, b the 9-story RC MRF in pounding condition including NPL record subset for SD of 1.0D

respectively, and for the performance level of C, the 3St-9RC-1 condition has the highest increase, i.e. by 27.03% (from 0.529 to 0.672). Therefore, the best model to enhance the performance levels of the 9-story RC MRF is 3St-9RC-4 and 3St-9RC-1 according to the condition defined in Table 4. It can also be seen that adding LVDs does not have a significant effect on M-IDAs of the 3-story SMRF. Although in previous models of pounding between the 3-story SMRF and 3-, and 5-story RC MRF, the M-IDAs of the 3-story SMRF significant reduction was obtained, pounding between the 3-story SMRF and the 9-story RC MRF has smaller effect on M-IDAs of the 3-story SMRF. Therefore, by increasing the height of the adjacent structure, M-IDAs of the 3-story SMRF will have fewer changes. Table 10 provides information on M-IDAs of the 3-story SMRF in detail. The results can also be used for retrofitting both adjacent structures. For example, if the 3St-9RC-4 condition is selected for retrofitting the 9-story RC MRF adjacent to the 3-story SMRF, it will have a significant influence on M-IDAs of the 9-story RC MRF according to the information presented in Table 10. On other side, it will increase M-IDAs of the 3-story SMRF in performance levels of IO and LS, while decreasing the values of performance levels of CP and C. In this condition in retrofitting, it is suggested to check and retrofit the adjacent structure for the performance levels of CP and C,

while it can be neglected in conservative way for other performances. It is worth noting that similar results were also observed for other record subsets.

3.6 Comparing M-IDAs of 5-story SMRF pounding with RC MRFs

Figure 14 presents the results of using LVDs on M-IDAs of the 5-story SMRF and the 5-story RC MRF subjected to NPL for SD of 1.0D. Using LVDs at all floor levels (5St-5RC-4) increases M-IDAs for the 5-story RC MRF by 30.3% (from 0.987 to 1.286) which is more than for other assumed models considering LVD at the 5th floor level (5St-5RC-1), at both 2nd and 5th floor levels (5St-5RC-2), and at the 1st, 3rd and 5th floor levels (5St-5RC-3) by 15.5%, 23.6%, and 21.3%, respectively. Therefore, the condition of 5St-5RC-4 is the best alternative to implement LVDs between structures. Table 11 presents details of M-IDAs of colliding structures in all performance levels. For the 5-story SMRF, the condition of 5St-5RC-1 is a better alternative due to the fact that it increases M-IDAs of the 5-story SMRF in IO and LS by 19.2% and 12.2%, respectively, while it decreases the values of CP and C by 1.5% and 0.39%, respectively. It can be seen that the reduction values of performance levels of CP and C do not significantly influence M-IDAs of the 5-story SMRF.

Table 10 Limited state capacities of the 3-story SMRF and the 9-story RC MRF subjected to NPL record subsets for SD of 1.0D

Model name	3-Story SMRF				9-Story RC MRF			
	IO	LS	CP	C	IO	LS	CP	C
3St-9RC-SD1.0D	0.229	0.806	1.373	1.892	0.164	0.289	0.449	0.529
3St-9RC-1-VD 1.0-SD1.0D	0.263	0.815	1.285	1.891	0.167	0.289	0.501	0.672
3St-9RC-2-VD 1.0-SD1.0D	0.286	0.884	1.342	1.850	0.170	0.291	0.494	0.656
3St-9RC-3-VD 1.0-SD1.0D	0.291	0.845	1.328	1.802	0.172	0.294	0.499	0.664
3St-9RC-4-VD 1.0-SD1.0D	0.299	0.865	1.344	1.806	0.173	0.295	0.506	0.662

Bold values indicate the best results obtained from implementing VDs

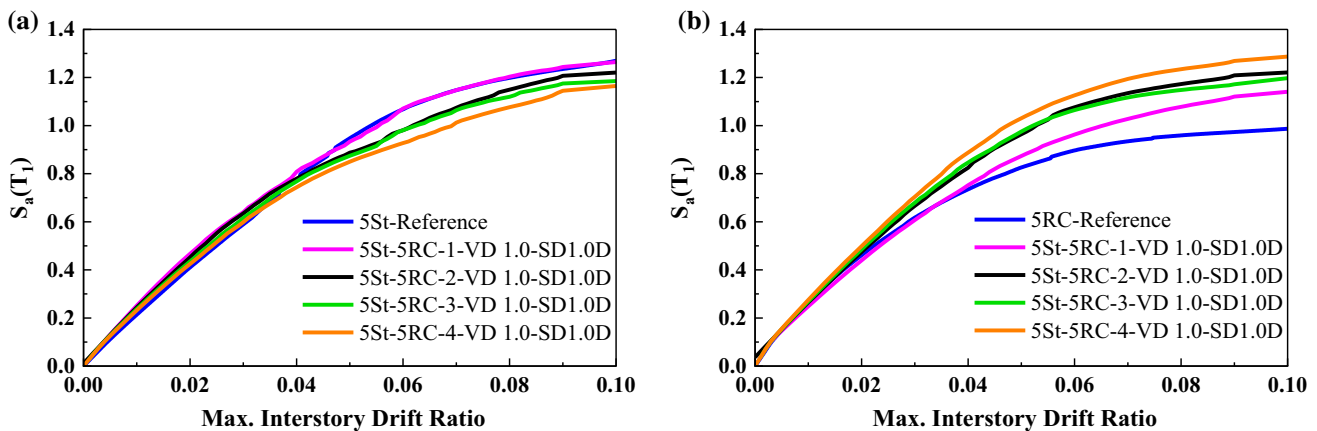


Fig. 14 Comparison M-IDAs of **a** the 5-story SMRF, **b** the 5-story RC MRF in pounding condition including NPL record subset for SD of 1.0D

For retrofitting purposes, using condition of 5St-5RC-4 can be the best suggestion for the 5-story RC MRF due to its increasing effects in all performance levels, but it should be said that this condition has a reduction effect on the CP and C performances of the 5-story SMRF. Therefore, it is suggested to check and retrofit the adjacent structure for the CP and C performances.

Figure 15 presents the results of using LVDs on M-IDAs of the 5-story SMRF and the 5-story RC MRF subjected to NNP for SD of 0.0. Using LVDs in all floor levels (5St-5RC-4) increases M-IDAs for the 5-story RC MRF by 59.6% (from 0.987 to 1.575) which is more than for other assumed models considering LVD at the 5th floor level (5St-5RC-1), at both 2nd and 5th floor levels (5St-5RC-2), and at the 1st, 3rd and 5th floor levels (5St-5RC-3) by 40.4%, 48.3%, and 48.3%, respectively. It can be noted that by decreasing the

SD from 1.0 to 0.0, the performance of LVDs implemented at all floor levels (5St-5RC-4) between the 5-story SMRF and the 5-story RC MRF increases by 37.71% (from 23.25% for SD of 1.0 to 37.33% for SD of 0.0). Therefore, this strategy is more useful to retrofit the 5-story RC MRF in any adjacency condition. Table 12 presents details of M-IDAs of colliding structures in all performance levels.

For the 5-story SMRF, the condition of 5St-5RC-3 is a better alternative due to the increased M-IDAs of the 5-story SMRF in performance levels of IO, LS, and CP by 5.9%, 13.2%, and 1.86%, respectively, while it decreases the value of performance level of C by 0.39%. According to retrofitting criteria (Seismic Evaluation and Retrofit of Existing Buildings), there were some retrofitting purposes that the designer regarding the knowledge about the structure can choose for a building to check them. Most of the purposes of retrofitting

Table 11 Limited state capacities of the 5-story SMRF and the 5-story RC MRF subjected to NPL record subsets for SD of 1.0D

Model name	5-Story SMRF				5-Story RC MRF			
	IO	LS	CP	C	IO	LS	CP	C
5St-5RC-SD1.0D	0.151	0.501	0.947	1.269	0.265	0.461	0.734	0.987
5St-5RC-1-VD 1.0-SD1.0D	0.180	0.562	0.933	1.264	0.248	0.439	0.752	1.140
5St-5RC-2-VD 1.0-SD1.0D	0.176	0.552	0.887	1.220	0.264	0.474	0.824	1.220
5St-5RC-3-VD 1.0-SD1.0D	0.172	0.528	0.874	1.185	0.268	0.485	0.846	1.197
5St-5RC-4-VD 1.0-SD1.0D	0.168	0.515	0.849	1.165	0.275	0.498	0.887	1.286

Bold values indicate the best results obtained from implementing VDs

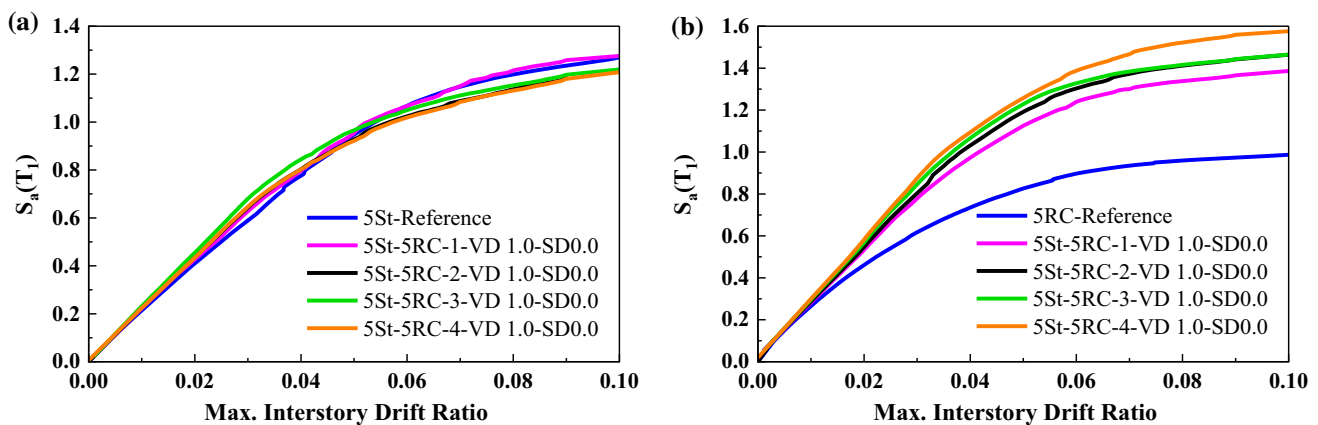


Fig. 15 Comparison M-IDAs of **a** the 5-story SMRF, **b** the 5-story RC MRF in pounding condition including NNP record subset for SD of 0.0

Table 12 Limited state capacities of the 5-story SMRF and the 5-story RC MRF subjected to NNP record subsets for SD of 0.0D

model name	5-Story SMRF				5-Story RC MRF			
	IO	LS	CP	C	IO	LS	CP	C
5St-5RC-SD0.0D	0.153	0.501	0.947	1.269	0.265	0.461	0.734	0.987
5St-5RC-1-VD 1.0-SD0.0D	0.156	0.522	0.953	1.275	0.282	0.533	0.972	1.386
5St-5RC-2-VD 1.0-SD0.0D	0.157	0.541	0.927	1.220	0.287	0.547	1.031	1.464
5St-5RC-3-VD 1.0-SD0.0D	0.162	0.567	0.965	1.219	0.296	0.567	1.066	1.464
5St-5RC-4-VD 1.0-SD0.0D	0.159	0.543	0.921	1.208	0.299	0.582	1.094	1.575

Bold values indicate the best results obtained from implementing VDs

are directed to achieve the performance levels of IO and LS. Therefore, in these performance levels, the designer should consider both structures' performances to assure choosing the best alternative in implementing the LVDs between the structures. In addition, the designer can choose the condition of 5St-5RC-1 regarding the details presented in Table 12. In this condition, although the performance levels of the 5-story SMRF were more or less unchanged (fluctuating between +4.02% and -0.47%), the performance levels of IO, LS, CP, and C for the 5-story RC MRF increased by 6.4%, 15.6%, 32.4%, and 40.4%, respectively.

Figure 16 presents the results of using LVDs on M-IDAs of the 5-story SMRF and the 9-story RC MRF subjected to NPL for SD of 1.0D. Using LVDs at both 2nd and 5th floor levels (5St-9RC-2) can be a good alternative for the 9-story RC MRF that causes a reduction in performance levels of IO and LS by 4.3% and 6.6%, respectively, while increasing the performance levels of CP and C by 2.39% and 23.3%, respectively. Other conditions of considering LVD at 5th floor level (5St-9RC-1), at the 1st, 3rd, and 5th floor levels (5St-9RC-3), and at all floor levels (5St-9RC-4) increase M-IDAs for the 9-story RC MRF by 6.8%, 11.9%, and 12.9%, respectively. Table 13

presents details of M-IDAs of colliding structures in all performance levels.

For the 5-story SMRF, the conditions of 5St-9RC-3 and 5St-9RC-4 are better alternatives due to increasing M-IDAs of the 5-story SMRF in performance levels of IO and LS by 30.1% and 10.2%, respectively. While for other performance levels, the conditions of 5St-9RC-1 can be chosen that decrease the values of the performance level of CP and C by 6.8% and 5.59%, respectively, less than for other conditions. Table 13 presents useful information concerning retrofitting these two adjacent structures. For example, the designer can decide to choose one of the conditions to implement the LVDs between the structures relying on the details provided in Table 13 and checking the effects of retrofitting one structure (e.g. the 5-story SMRF) on the other one (e.g. the 9-story RC MRF).

3.7 Comparing M-IDAs of 9-story SMRF pounding with RC MRFs

Figure 17 presents the results of using LVDs on M-IDAs of the 9-story SMRF and the 3-story RC MRF subjected to NPL for SD of 0.0. Using LVDs at all floor levels (9St-3RC-4) increases M-IDAs for the 3-story RC MRF in

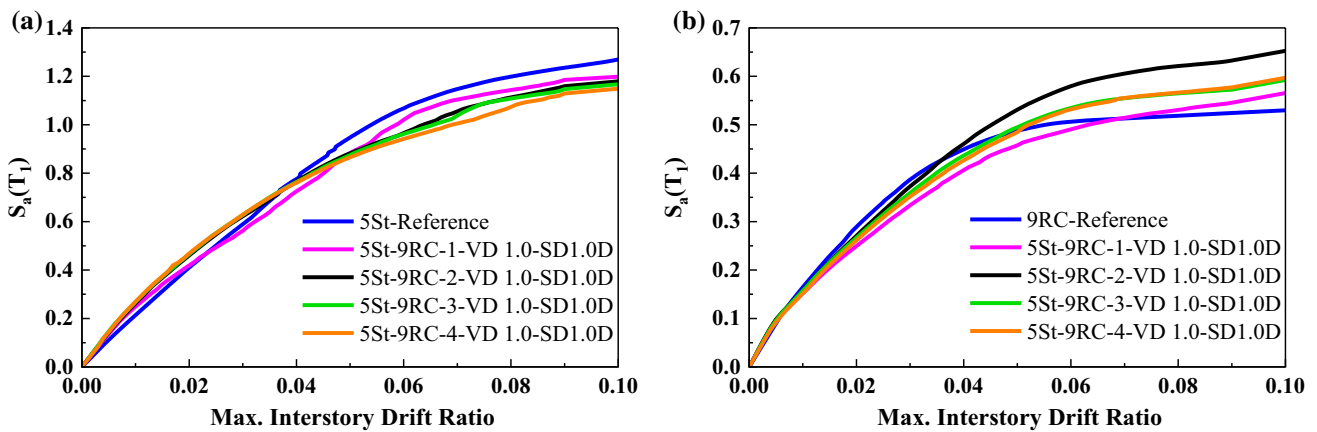


Fig. 16 Comparison M-IDAs of a) the 5-story SMRF, b) the 9-story RC MRF in pounding condition including NPL record subset for SD of 1.0D

Table 13 Limited state capacities of the 5-story SMRF and 9-story RC MRF subjected to NPL record subsets for SD of 1.0D

Model name	5-Story SMRF				9-Story RC MRF			
	IO	LS	CP	C	IO	LS	CP	C
5St-9RC-SD1.0D	0.153	0.501	0.947	1.269	0.164	0.289	0.449	0.529
5St-9RC-1-VD 1.0-SD1.0D	0.187	0.493	0.883	1.198	0.151	0.249	0.406	0.565
5St-9RC-2-VD 1.0-SD1.0D	0.193	0.546	0.881	1.179	0.157	0.270	0.460	0.652
5St-9RC-3-VD 1.0-SD1.0D	0.199	0.552	0.875	1.167	0.156	0.266	0.436	0.592
5St-9RC-4-VD 1.0-SD1.0D	0.199	0.552	0.865	1.149	0.151	0.261	0.426	0.597

Bold values indicate the best results obtained from implementing VDs

performance levels of IO, LS, CP, and C by 11.2%, 18%, 42.5%, and 32.8%, respectively. Moreover, other conditions of considering LVD at the 2nd floor level (9St-3RC-1), at the 3rd floor level (9St-3RC-2), and at the 1st and 3rd floor levels (9St-3RC-3) increase M-IDAs for the 3-story RC MRF by 16.7%, 19.9%, and 7.3%, respectively. Table 14 presents details of M-IDAs of colliding structures in all performance levels. For the 9-story SMRF, the conditions of 9St-3RC-3 and 9St-3RC-1 are better alternatives due to increasing

M-IDAs of the 9-story SMRF in performance levels of IO and LS by 30.4% and 8%, respectively, and increasing the performance levels of CP and C by 21.1% and 36%, respectively. Although using the condition of (9St-3RC-4) is the best alternative for the 3-story RC MRF, this condition also stands in the second rate for the 9-story SMRF. Therefore, according to Table 14, for retrofitting purposes, the designer can decide to choose one of the conditions to implement the LVDs between the structures.

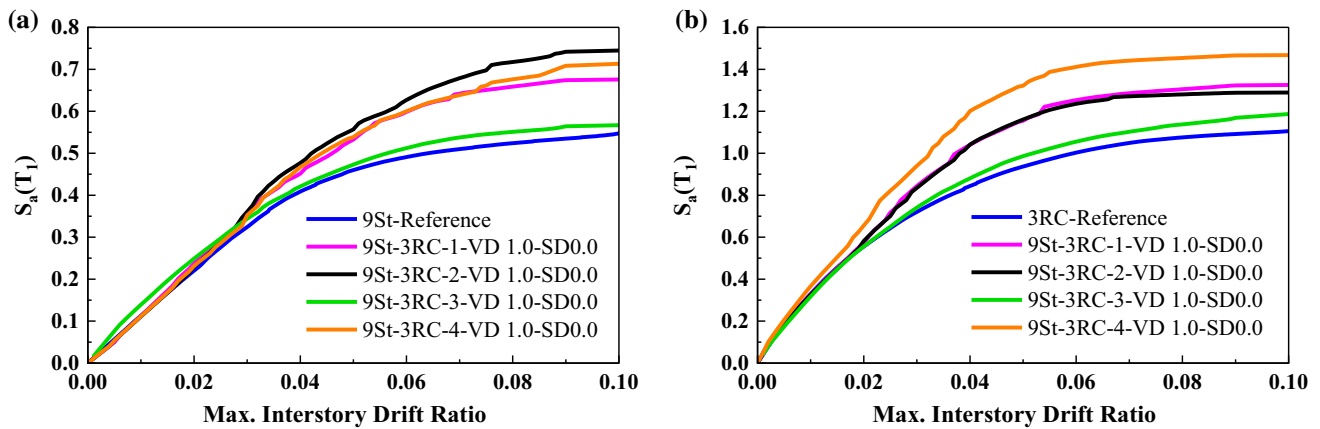


Fig. 17 Comparison M-IDAs of a) the 9-story SMRF, b) the 3-story RC MRF in pounding condition including NPL record subset for SD of 0.0

Table 14 Limited state capacities of the 9-story SMRF and 3-story RC MRF subjected to NPL record subsets for SD of 0.0D

Model name	9-Story SMRF				3-Story RC MRF			
	IO	LS	CP	C	IO	LS	CP	C
9St-3RC-SD0.0D	0.079	0.275	0.459	0.547	0.329	0.555	0.843	1.105
9St-3RC-1-VD 1.0-SD0.0D	0.076	0.284	0.556	0.744	0.325	0.581	1.041	1.289
9St-3RC-2-VD 1.0-SD0.0D	0.076	0.283	0.532	0.675	0.328	0.574	1.040	1.325
9St-3RC-3-VD 1.0-SD0.0D	0.103	0.297	0.472	0.566	0.317	0.555	0.880	1.186
9St-3RC-4-VD 1.0-SD0.0D	0.079	0.285	0.538	0.713	0.366	0.655	1.201	1.467

Bold values indicate the best results obtained from implementing VDs

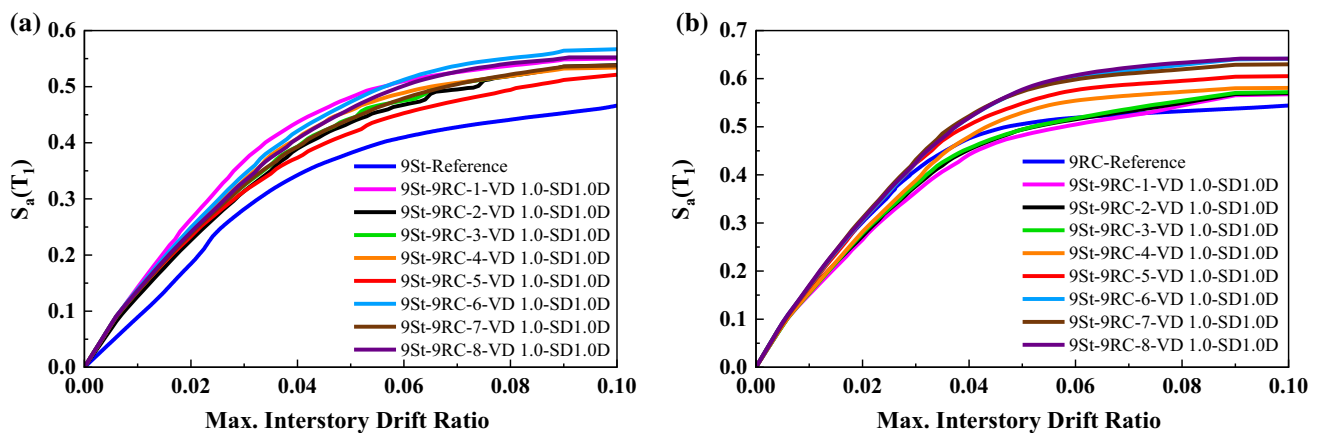


Fig. 18 Comparison M-IDAs of a) the 9-story SMRF, b) the 9-story RC MRF in pounding condition including NPL record subset for SD of 1.0D

Table 15 Limited state capacities of the 9-story SMRF and 9-story RC MRF structures subjected to NPL record subsets for SD of 1.0D

Model name	9-Story RC MRF				9-Story SMRF			
	IO	LS	CP	C	IO	LS	CP	C
9St-9RC-SD1.0D	0.062	0.242	0.381	0.466	0.166	0.301	0.475	0.544
9St-9RC-1-VD 1.0-SD1.0D	0.103	0.317	0.480	0.550	0.151	0.265	0.442	0.567
9St-9RC-2-VD 1.0-SD1.0D	0.094	0.271	0.436	0.538	0.157	0.272	0.452	0.569
9St-9RC-3-VD 1.0-SD1.0D	0.102	0.281	0.443	0.536	0.154	0.278	0.455	0.572
9St-9RC-4-VD 1.0-SD1.0D	0.103	0.289	0.457	0.534	0.155	0.281	0.479	0.581
9St-9RC-5-VD 1.0-SD1.0D	0.102	0.275	0.417	0.521	0.165	0.304	0.503	0.605
9St-9RC-6-VD 1.0-SD1.0D	0.103	0.297	0.472	0.566	0.168	0.305	0.519	0.641
9St-9RC-7-VD 1.0-SD1.0D	0.101	0.282	0.442	0.537	0.170	0.310	0.522	0.629
9St-9RC-8-VD 1.0-SD1.0D	0.103	0.286	0.460	0.553	0.168	0.307	0.518	0.649

Bold values indicate the best results obtained from implementing VDs

Figure 18 presents the results of using LVDs on M-IDAs of the 9-story SMRF and the 9-story RC MRF subjected to NPL for SD of 1.0D. Implementing LVDs at the floor levels of the 1st, 3rd, 5th, 7th, and 9th (9St-9RC-7) increases M-IDAs for the 9-story RC MRF in performance levels of IO, LS, and CP by 2.4%, 2.9%, and 9.9%, respectively. While for the performance level of C, the condition of 9St-9RC-8 increases M-IDAs for the 9-story RC MRF by 19.3%, which is more than for other conditions. Table 15 presents details of M-IDAs of colliding structures in all performance levels.

For the 9-story SMRF, all the conditions increase the amount of M-IDAs and they can be chosen for retrofitting purposes. The conditions of 9St-9RC-1, 9St-9RC-4, 9St-9RC-6, and 9St-9RC-8 are good alternatives to increase the performance level of IO by 66.1%. The only difference between them is the cost of implementation of LVDs. In the condition of 9St-9RC-1, only one LVD at the top floor can increase M-IDAs of the 9-story SMRF in the performance level of IO by the same value as in the case of other conditions (e.g. 9St-9RC-4, 9St-9RC-6,

and 9St-9RC-8) with a lower cost of the implementation. In addition, the condition of 9St-9RC-1 is the best alternative for increasing the performance levels of LS and CP by 31% and 26%, respectively. Moreover, the condition of 9St-9RC-6 increases the performance level of C by 21.5%. It can be noted that using Table 15 can help designers to choose and compare the alternatives of adding LVDs between the structures by considering the amount of increased values of performance levels and the cost of the implementation. Also, it is suggested that the performance levels of the adjacent structure should be checked based on the influence of adding LVDs that were presented in the figures.

4 Seismic failure probability

To evaluate the effects of implemented VDs, the seismic fragility curves were plotted for the performance level of C. Figure 19 illustrates the seismic fragility curves of the

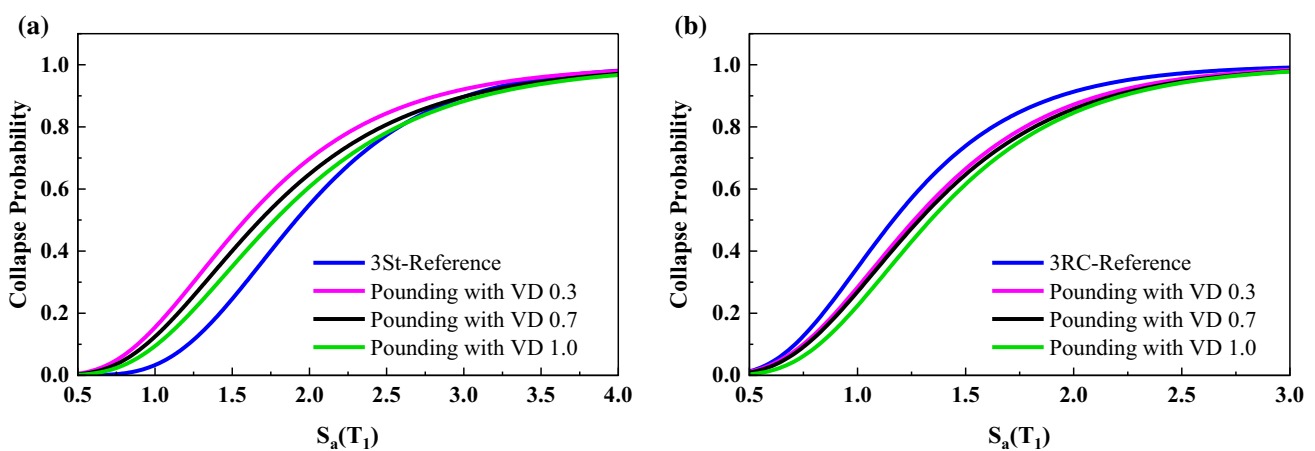


Fig. 19 Seismic fragility curves of **a** the 3-story SMRF, **b** the 3-story RC MRF assuming implemented NVDs or LVDs in second story level including NNP record subset for SD of 1.0D

3-story SMRF and RC MRF with different types of VDs implemented on second story level including NNP records given SD of 1.0D. The $S_a(T_1)$ corresponding to the failure probability of 50% for the 3-story SMRF in the performance level of C assuming VDs with damper velocity exponent of 0.3, 0.7, and 1.0 were determined by 1.61, 1.71, and 1.79, respectively, in which, the LVDs achieved higher values of $S_a(T_1)$ that shows the lower value of the failure probability. On the other side, the $S_a(T_1)$ corresponding to the failure probability of 50% for the 3-story RC MRF in the performance level of C assuming VDs with damper velocity exponent of 0.3, 0.7, and 1.0 were determined by 1.27, 1.29, and 1.35, respectively. The results confirmed that the structures with implemented LVDs achieved higher values of $S_a(T_1)$ in the failure probability of 50%.

Figures 20 and 21 illustrate the seismic fragility curves of the 3-story and 5-story SMRFs colliding with RC MRFs

of similar height assuming different types of implementing VDs including NNP and NPL records and SD of 1.0D, respectively. It is obvious that adding LVDs can significantly decrease the seismic failure probability of RC MRFs, while it can increase the seismic failure probability of SMRFs. Therefore, it can be concluded that different types of lateral resisting systems can affect the results of implementing VDs between the adjacent structures with similar heights. In addition, implementing VDs in all story levels can be the best alternative for retrofitting the RC MRFs, while this condition can significantly increase the seismic failure probability of SMRFs. Thus, it is recommended that the condition of adjacent structure should be considered in the retrofitting process.

Figures 22 and 23 illustrate the fragility curves of the 3-story SMRF and 5-story RC MRF, and the 5-story SMRF and 9-story RC MRF including NNP records and SD of

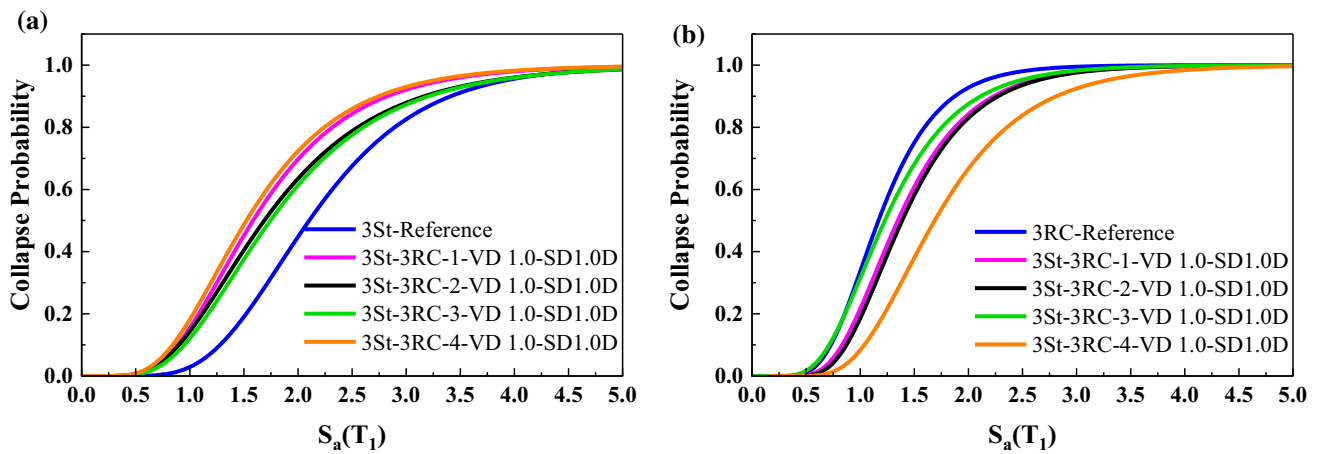


Fig. 20 Seismic fragility curves of **a** the 3-story SMRF, **b** the 3-story RC MRF in pounding condition including NNP record subset for SD of 1.0D

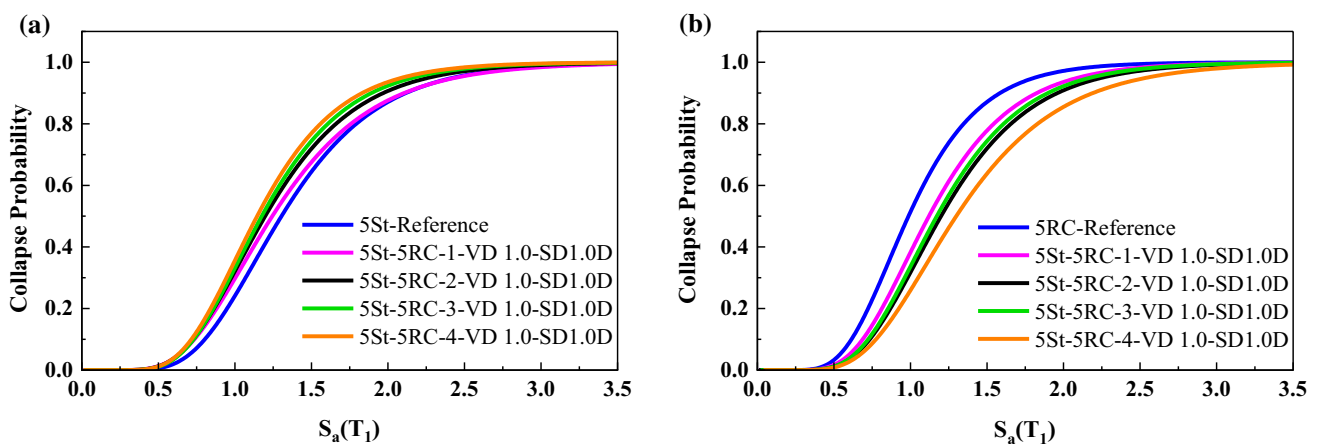


Fig. 21 Seismic fragility curves of **a** the 5-story SMRF, **b** the 5-story RC MRF in pounding condition including NPL record subset for SD of 1.0D

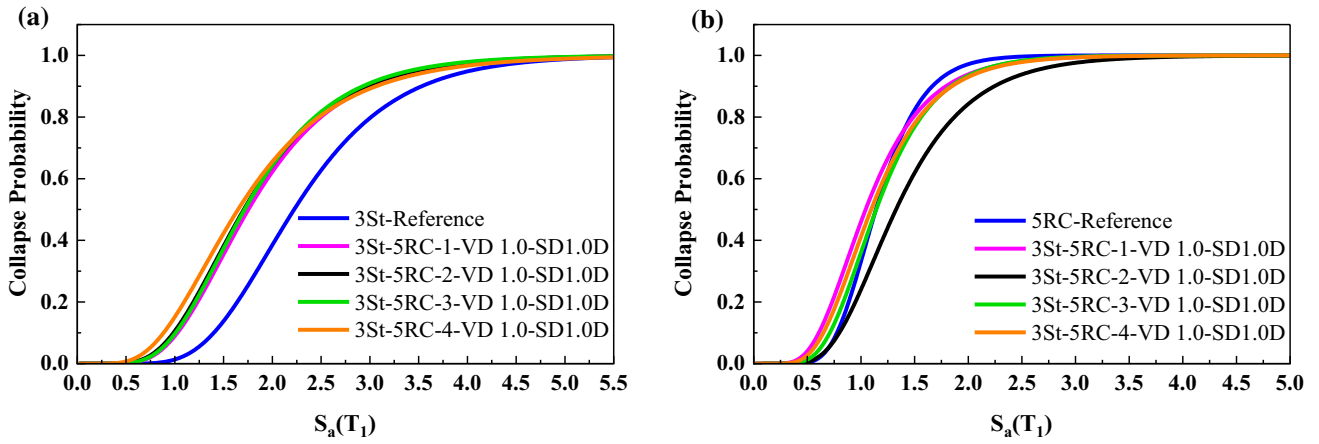


Fig. 22 Seismic fragility curves of a the 3-story SMRF, b the 5-story RC MRF in pounding condition including NNP record subset for SD of 1.0D

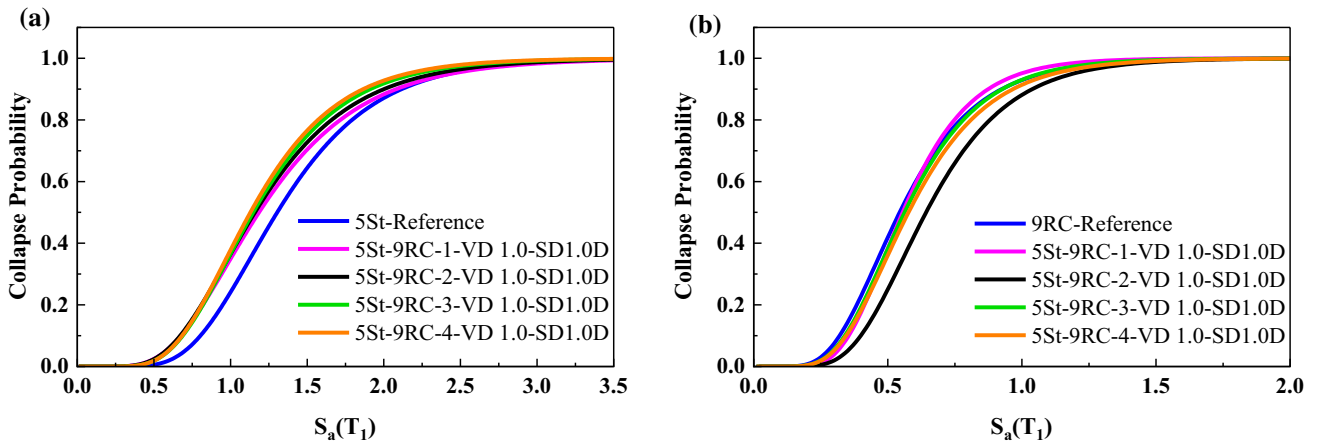


Fig. 23 Seismic fragility curves of a the 5-story SMRF, b the 9-story RC MRF in pounding condition including NNP record subset for SD of 1.0D

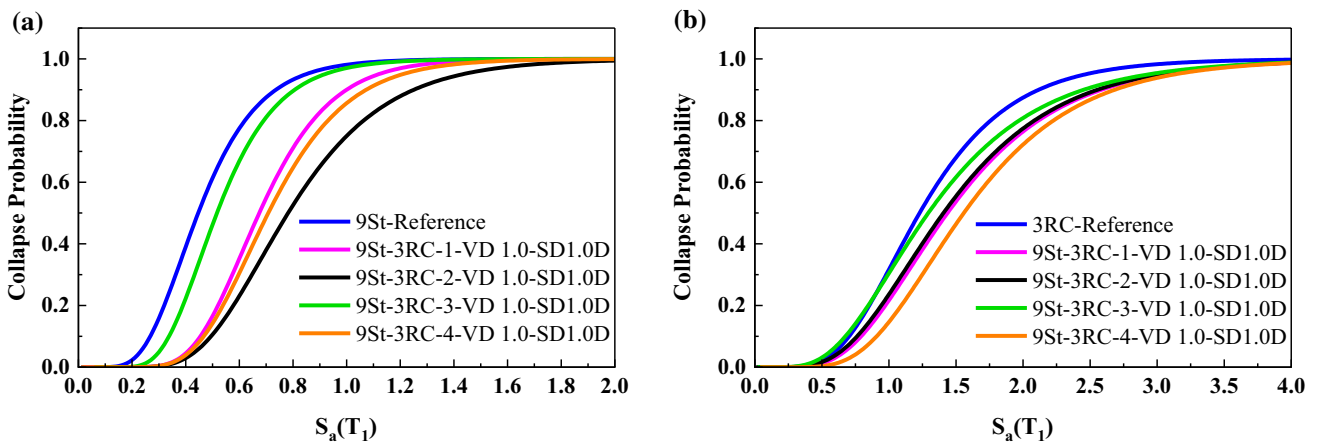


Fig. 24 Seismic fragility curves of a the 9-story SMRF, b the 3-story RC MRF in pounding condition including NNP record subset for SD of 0.0

1.0D, respectively. It is presented that implementing VDs can increase the failure probability of shorter structures (i.e. the 3-, and 5-story SMRFs), while the failure probability of taller structure remains more or less unchanged, except for placement of condition two (see Table 4). In the case of pounding between taller and shorter structures, results of failure probability for the 9-story SMRF and 3-story RC MRF, including NNP records for SD of 0.0, were compared in Fig. 24. It can be observed from the figure that implementing VDs in this condition can help both structures and improve their failure probabilities. It can be said that, due to possibility of collapse in the middle of the 9-story SMRF, implementing the VD in the top floor of the 3-story RC MRF prevents the failure of the 9-story SMRF; then, as a result,

the failure probability is reduced. On the other hand, this situation helped the 3-story RC MRF to decrease the failure probability.

5 Retrofitting modification factors

Based on the results concerning the M-IDAs of colliding structures, Retrofitting Modification Factors (RMFs) were calculated after dividing the M-IDAs of the colliding structures in the retrofitted condition (presented in Table 4) by the corresponding values of M-IDAs without any retrofitting devices (e.g. VDs). The RMFs can be applied to the structures with the same conditions and structural elements

Table 16 RMF of the 3-story SMRF and the 3-story RC MRF subjected to all record subsets for SD of 0.0 and 1.0D

Model name	SD	3-Story SMRF				3-Story RC MRF			
		IO	LS	CP	C	IO	LS	CP	C
3St-3RC-1-VD 1.0	1.0D	1.000	0.878	0.821	0.855	1.036	1.076	1.110	1.124
	0.0	0.997	0.869	0.816	0.848	1.029	1.068	1.105	1.119
3St-3RC-2-VD 1.0	1.0D	0.969	0.831	0.888	0.946	0.842	0.908	0.972	1.134
	0.0	0.960	0.823	0.875	0.940	0.834	0.898	0.967	1.129
3St-3RC-3-VD 1.0	1.0D	1.140	0.927	0.876	0.938	0.964	1.000	1.044	1.073
	0.0	1.138	0.921	0.871	0.931	0.958	0.993	1.038	1.067
3St-3RC-4-VD 1.0	1.0D	1.052	0.880	0.824	0.838	1.079	1.114	1.185	1.325
	0.0	1.049	0.874	0.817	0.831	1.071	1.107	1.178	1.319

Table 17 RMF of the 3-story SMRF and the 5-story RC MRF subjected to all record subsets for SD of 0.0 and 1.0D

Model name	SD	3-Story SMRF				5-Story RC MRF			
		IO	LS	CP	C	IO	LS	CP	C
3St-5RC-1-VD 1.0	1.0D	1.170	1.048	0.867	0.923	0.883	0.892	0.993	1.054
	0.0	1.167	1.052	0.873	0.921	0.889	0.899	1.003	1.059
3St-5RC-2-VD 1.0	1.0D	0.983	0.865	0.714	0.898	0.974	1.007	1.114	1.268
	0.0	0.985	0.869	0.719	0.905	0.978	1.014	1.119	1.276
3St-5RC-3-VD 1.0	1.0D	1.004	0.903	0.755	0.952	0.936	0.961	1.030	1.138
	0.0	1.000	0.896	0.750	0.948	0.930	0.965	1.035	1.145
3St-5RC-4-VD 1.0	1.0D	1.048	0.918	0.763	0.879	0.928	0.937	1.018	1.124
	0.0	1.046	0.915	0.758	0.875	0.923	0.938	1.022	1.128

Table 18 RMF of the 3-story SMRF and the 9-story RC MRF subjected to all record subsets for SD of 0.0 and 1.0D

Model name	SD	3-Story SMRF				9-Story RC MRF			
		IO	LS	CP	C	IO	LS	CP	C
3St-9RC-1-VD 1.0	1.0D	1.148	1.011	0.936	0.999	1.018	1.000	1.116	1.270
	0.0	1.155	1.017	0.944	1.021	1.010	0.998	1.115	1.268
3St-9RC-2-VD 1.0	1.0D	1.249	1.097	0.977	0.978	1.037	1.007	1.100	1.240
	0.0	1.245	1.090	0.979	0.988	1.044	1.015	1.110	1.251
3St-9RC-3-VD 1.0	1.0D	1.271	1.048	0.967	0.952	1.049	1.017	1.111	1.255
	0.0	1.266	1.044	0.960	0.945	1.048	1.014	1.106	1.250
3St-9RC-4-VD 1.0	1.0D	1.306	1.073	0.979	0.955	1.055	1.021	1.127	1.251
	0.0	1.300	1.067	0.970	0.947	1.059	1.028	1.129	1.258

Table 19 RMF of the 5-story SMRF and the 3-story RC MRF subjected to all record subsets for SD of 0.0 and 1.0D

Model name	SD	5-Story SMRF				3-Story RC MRF			
		IO	LS	CP	C	IO	LS	CP	C
5St-3RC-1-VD 1.0	1.0D	1.192	1.122	0.985	0.996	0.936	0.952	1.025	1.155
	0.0	1.188	1.118	0.989	0.999	0.933	0.960	1.032	1.161
5St-3RC-2-VD 1.0	1.0D	1.166	1.102	0.937	0.961	0.996	1.028	1.123	1.236
	0.0	1.161	1.002	0.944	0.967	0.990	1.032	1.126	1.239
5St-3RC-3-VD 1.0	1.0D	1.139	1.054	0.923	0.934	1.011	1.052	1.153	1.213
	0.0	1.136	1.040	0.934	0.944	1.003	1.062	1.156	1.219
5St-3RC-4-VD 1.0	1.0D	1.113	1.028	0.897	0.918	1.038	1.080	1.208	1.303
	0.0	1.109	1.027	0.902	0.926	1.033	1.072	1.198	1.295

Table 20 RMF of the 5-story SMRF and the 5-story RC MRF subjected to all record subsets for SD of 0.0 and 1.0D

Model name	SD	5-Story SMRF				5-Story RC MRF			
		IO	LS	CP	C	IO	LS	CP	C
5St-5RC-1-VD 1.0	1.0D	1.020	1.042	1.006	1.005	1.064	1.156	1.324	1.404
	0.0	1.025	1.044	1.010	1.011	1.066	1.159	1.329	1.409
5St-5RC-2-VD 1.0	1.0D	1.026	1.080	0.979	0.961	1.083	1.187	1.405	1.483
	0.0	1.027	1.088	0.983	0.965	1.088	1.191	1.409	1.486
5St-5RC-3-VD 1.0	1.0D	1.059	1.132	1.019	0.961	1.117	1.230	1.452	1.483
	0.0	1.061	1.135	1.022	0.965	1.120	1.233	1.455	1.486
5St-5RC-4-VD 1.0	1.0D	1.039	1.084	0.973	0.952	1.128	1.262	1.490	1.596
	0.0	1.043	1.088	0.979	0.958	1.133	1.266	1.492	1.599

Table 21 RMF of the 5-story SMRF and the 9-story RC MRF subjected to all record subsets for SD of 0.0 and 1.0D

Model name	SD	5-Story SMRF				9-Story RC MRF			
		IO	LS	CP	C	IO	LS	CP	C
5St-9RC-1-VD 1.0	1.0D	1.222	0.984	0.932	0.944	0.921	0.862	0.904	1.068
	0.0	1.220	0.988	0.936	0.946	0.922	0.865	0.908	1.072
5St-9RC-2-VD 1.0	1.0D	1.261	1.090	0.930	0.929	0.957	0.934	1.024	1.233
	0.0	1.256	1.099	0.937	0.933	0.961	0.937	1.028	1.238
5St-9RC-3-VD 1.0	1.0D	1.301	1.102	0.924	0.920	0.951	0.920	0.971	1.119
	0.0	1.298	1.106	0.927	0.924	0.956	0.922	0.976	1.122
5St-9RC-4-VD 1.0	1.0D	1.301	1.102	0.913	0.905	0.921	0.903	0.949	1.129
	0.0	1.293	1.06	0.916	0.908	0.925	0.908	0.953	1.133

Table 22 RMF of the 9-story SMRF and the 3-story RC MRF subjected to all record subsets for SD of 0.0 and 1.0D

Model name	SD	9-Story SMRF				3-Story RC MRF			
		IO	LS	CP	C	IO	LS	CP	C
9St-3RC-1-VD 1.0	1.0D	0.962	1.033	1.211	1.360	0.988	1.047	1.235	1.167
	0.0	0.966	1.036	1.217	1.362	0.993	1.052	1.239	1.171
9St-3RC-2-VD 1.0	1.0D	0.962	1.029	1.159	1.234	0.997	1.034	1.234	1.199
	0.0	0.966	1.035	1.167	1.237	1.008	1.039	1.238	1.205
9St-3RC-3-VD 1.0	1.0D	1.304	1.080	1.028	1.035	0.964	1.000	1.044	1.073
	0.0	1.308	1.085	1.032	1.037	0.969	0.993	1.038	1.068
9St-3RC-4-VD 1.0	1.0D	1.000	1.036	1.172	1.303	1.112	1.180	1.425	1.328
	0.0	0.993	1.039	1.177	1.305	1.119	1.174	1.420	1.323

Table 23 RMF of the 9-story SMRF and the 5-story RC MRF subjected to all record subsets for SD of 0.0 and 1.0D

Model name	SD	9-Story SMRF				5-Story RC MRF			
		IO	LS	CP	C	IO	LS	CP	C
9St-5RC-1-VD 1.0	1.0D	0.977	1.102	1.126	1.129	0.908	1.117	1.247	1.178
	0.0	0.982	1.109	1.129	1.135	0.917	1.123	1.254	1.184
9St-5RC-2-VD 1.0	1.0D	0.950	1.003	1.212	1.108	0.999	1.056	1.235	1.201
	0.0	0.957	1.005	1.208	1.116	1.009	1.065	1.242	1.208
9St-5RC-3-VD 1.0	1.0D	1.211	1.121	1.045	1.110	0.989	1.023	1.078	1.088
	0.0	1.208	1.127	1.049	1.117	0.994	1.029	1.083	1.094
9St-5RC-4-VD 1.0	1.0D	1.130	1.250	1.081	1.124	1.108	1.230	1.455	1.342
	0.0	1.125	1.255	1.089	1.129	1.111	1.234	1.459	1.347

Table 24 RMF of the 9-story SMRF and the 9-story RC MRF subjected to all record subsets for SD of 0.0 and 1.0D

Model name	SD	9-Story SMRF				9-story RC MRF			
		IO	LS	CP	C	IO	LS	CP	C
9St-9RC-1-VD 1.0	1.0D	1.661	1.310	1.260	1.180	0.910	0.880	0.931	1.042
	0.0	1.668	1.312	1.266	1.189	0.918	0.888	0.933	1.040
9St-9RC-2-VD 1.0	1.0D	1.516	1.120	1.144	1.155	0.946	0.904	0.952	1.046
	0.0	1.508	1.122	1.149	1.159	0.951	0.911	0.956	0.044
9St-9RC-3-VD 1.0	1.0D	1.645	1.161	1.163	1.150	0.928	0.924	0.958	1.051
	0.0	1.649	1.163	1.166	1.148	0.927	0.929	0.962	1.049
9St-9RC-4-VD 1.0	1.0D	1.661	1.194	1.199	1.146	0.934	0.934	1.008	1.068
	0.0	1.668	1.197	1.203	1.147	0.933	0.938	1.018	1.067
9St-9RC-5-VD 1.0	1.0D	1.645	1.136	1.094	1.118	0.994	1.010	1.059	1.112
	0.0	1.649	1.138	1.099	1.121	0.999	1.014	1.066	1.110
9St-9RC-6-VD 1.0	1.0D	1.661	1.227	1.239	1.215	1.012	1.013	1.093	1.178
	0.0	1.668	1.232	1.244	1.219	1.018	1.017	1.099	1.169
9St-9RC-7-VD 1.0	1.0D	1.629	1.165	1.160	1.152	1.024	1.030	1.099	1.156
	0.0	1.631	1.169	1.163	1.163	1.033	1.038	1.103	1.155
9St-9RC-8-VD 1.0	1.0D	1.661	1.182	1.207	1.187	1.012	1.020	1.091	1.193
	0.0	1.668	1.185	1.213	1.196	1.019	1.028	1.098	1.195

to help designers approximately calculate the performance levels of the colliding structures when using LVDs. RMFs can be used for all kinds of assumed structures and aforementioned SDs. According to the results for different record subsets, the difference between the performance levels of M-IDAs for the colliding structures with and without retrofitting devices are approximately equal. Therefore, RMFs can be successfully used for colliding structures subjected to three aforementioned record subsets. In addition, RMFs can help designers to estimate the amount of M-IDAs after retrofitting. To calculate RMFs, the pounding model and the condition of retrofitting according to the Table 4 should be firstly selected. Then the values obtained from Tables 16, 17, 18, 19, 20, 21, 22, 23 and 24 can be applied to the pounding condition of models. For example, for the condition of 9St-3RC-3 for SD of 1.0D, M-IDAs of the 9-story SMRF and 3-story RC MRF colliding structures should be multiplied by 1.035 and 1.073 (RMFs according to Table 22),

respectively, to achieve the performance level of C of the retrofitted structures.

6 Conclusions

This study has been focused on seismic limit-states of SMRFs and RC MRFs prone to earthquake-induced pounding. The effects of adding VDs between adjacent structures have been carried out and proper RMFs for retrofitting purposes have been determined assuming three SDs of 0.0, 0.5D, and 1.0D. In this study, a Tcl code was developed to assess the limit-state capacity of adjacent pounding structures taking into account the collapsed structure. The results are summarized as follows:

- The results confirm that pounding between adjacent structures can cause an increase in the maximum values of the moment-rotation curves of beams and columns

(e.g. beam and column of the 3-story SMRF colliding with 5-story RC MRF experienced an increase by 16% and 29.1%, respectively). The placement of LVDs between structures can be effective to reduce the values of the moment-rotation curves for beams and columns by 48% and 31.25%, respectively.

- Regarding RC MRFs and SMRFs without any adjacent structure, the values of M-IDAs for the IO, LS, CP, and C performance levels of RC MRFs including the NNP records were higher than for other subsets. While this was correct for the 3-story SMRF, in the case of 5-, and 9-story SMRFs, the assumed performance levels in the FF subset were higher than for other subsets.
- Comparing the results of using NVDs and LVDs, it can be seen that LVDs attain better performance levels, as compared to the NVDs, for three different record subsets and SDs.
- The results confirm that implementing LVDs between adjacent structures play a crucial role in increasing the performance levels of RC MRFs. For example, in the condition of 3St-3RC-4, M-IDAs for the 3-story RC MRF increased by 32.48%, in the condition of 3St-5RC-2, M-IDAs for the 5-story RC MRF increased by 26.8%, in the condition of 3St-9RC-1, M-IDAs for the 9-story RC MRF increased by 27.03%. Although RC MRFs achieved higher performance levels, the alternative conditions were caused by the reduction in M-IDAs of the 3-story SMRF. Therefore, it is suggested to consider both structures' performance levels in retrofitting approach and choose the best model according to required performance levels.
- RMFs were proposed to approximately predict the M-IDAs of the structures after retrofitting. The RMFs can be easily applied to the structures with the same structural elements to help designers approximately calculate the performance levels of the colliding structures when using LVDs between the structures without involving analytical difficulties.
- Comparing pounding between MRFs of similar height (i.e. the 3-, and 5-story) shows that adding VD's can significantly decrease the seismic failure probability of RC MRFs, while it can increase the seismic failure probability of SMRFs. The results confirm that implementing VD's can increase the failure probability of shorter structures (i.e. the 3-, and 5-story SMRFs), while the failure probability of taller structure remains more or less unchanged, except for placement of condition two. Comparing pounding between taller SMRF and shorter RC MRF shows that implementing the VD at the top of the shorter RC MRF prevents the failure of the taller SMRF; then, as a result, the failure probability is reduced.
- To address the reason behind this, it can be said that pounding phenomenon leads to complex situation that

any changes, such as lateral resisting system, total weight of structure, fundamental period, and implementing VD's, can affect the impact forces at the floor levels, which may change the seismic behavior of both structures. Therefore, it is recommended that the condition of adjacent structure should be considered in the retrofitting process of the building under investigation.

Author contributions All authors contributed to the study conception and design. Material preparation, data collection and analysis were performed by NA, FK, and RJ. The first draft of the manuscript was written by FK and all authors commented on previous versions of the manuscript. All authors read and approved the final manuscript. NA: Writing-original draft preparation, analysis, and investigation. FK: Methodology, Conceptualization, Writing. RJ: Review and editing, Supervision.

Declarations

Conflict of interest All authors declare that they have no conflict of interest.

Ethical approval This material is the authors' own original work, which has not been previously published elsewhere. The paper is not currently being considered for publication elsewhere. The paper reflects the authors' own research and analysis in a truthful and complete manner.

Open Access This article is licensed under a Creative Commons Attribution 4.0 International License, which permits use, sharing, adaptation, distribution and reproduction in any medium or format, as long as you give appropriate credit to the original author(s) and the source, provide a link to the Creative Commons licence, and indicate if changes were made. The images or other third party material in this article are included in the article's Creative Commons licence, unless indicated otherwise in a credit line to the material. If material is not included in the article's Creative Commons licence and your intended use is not permitted by statutory regulation or exceeds the permitted use, you will need to obtain permission directly from the copyright holder. To view a copy of this licence, visit <http://creativecommons.org/licenses/by/4.0/>.

References

1. Sołtysik B, Jankowski R. Non-linear strain rate analysis of earthquake-induced pounding between steel buildings. *Int J Earth Sci Eng*. 2013;6(3):429–33.
2. Elwardany H, Seleemah A, Jankowski R, El-Khoriby S. Influence of soil–structure interaction on seismic pounding between steel frame buildings considering the effect of infill panels. *Bull Earthq Eng*. 2019;17(11):6165–202.
3. Rezaei H, Moayyedi SA, Jankowski R. Probabilistic seismic assessment of RC box-girder highway bridges with unequal-height piers subjected to earthquake-induced pounding. *Bull Earthq Eng*. 2020;18(4):1547–78.
4. Kazemi F, Asgarkhani N, Manguri A, Jankowski R. Investigating an optimal computational strategy to retrofit buildings with implementing viscous dampers. *Int Conf Comput Sci ICCS Proc, Lecture Notes in Compu Sci*, vol. 13351. 2022. p. 184–91. https://doi.org/10.1007/978-3-031-08754-7_25.

5. Kazemi F, Mohebi B, Yakhchalian M. Predicting the seismic collapse capacity of adjacent structures prone to pounding. *Can J Civ Eng*. 2020;47(6):663–77.
6. Cole G, Dhakal RP, Carr AJ, Bull D. Building pounding state of the art: Identifying structures vulnerable to pounding damage. In: *Proceedings of New Zealand society for earthquake engineering annual conference*, 2010.
7. Kazemi F, Mohebi B, Yakhchalian M. Evaluation the P -delta effect on collapse capacity of adjacent structures subjected to far-field ground motions. *Civ Eng J*. 2018;4(5):1066. <https://doi.org/10.28991/cej-0309156>.
8. Favvata MJ. Minimum required separation gap for adjacent RC frames with potential inter-story seismic pounding. *Eng Struct*. 2017;152:643–59.
9. Mohebi B, Kazemi F, Yakhchalian M. Investigating the P -Delta effects on the seismic collapse capacity of adjacent structures. In: *16th European conference on earthquake engineering (16ECEE)*, 18–21, June, Thessaloniki, Greece, 2018.
10. Jankowski R. Experimental study on earthquake-induced pounding between structural elements made of different building materials. *Earthq Eng Struct Dyn*. 2010;39(3):343–54.
11. Leibovich E, Rutenberg A, Yankelevsky DZ. On eccentric seismic pounding of symmetric buildings. *Earthq Eng Struct Dyn*. 1996;25(3):219–33.
12. Polycarpou PC, Papalouizou L, Komodromos P. An efficient methodology for simulating earthquake-induced 3D pounding of buildings. *Earthq Eng Struct Dyn*. 2014;43(7):985–1003.
13. Skrekas P, Sextos A, Giaralis A. Influence of bi-directional seismic pounding on the inelastic demand distribution of three adjacent multi-storey R/C buildings. *Earthq Struct*. 2014;6(1):71–87.
14. Raheem SEA, Fooly MY, Shafy AGA, Taha AM, Abbas YA, Latif MMA. Numerical simulation of potential seismic pounding among adjacent buildings in series. *Bull Earthq Eng*. 2019;17(1):439–71.
15. Yahyazadeh A, Yakhchalian M. Probabilistic residual drift assessment of SMRFs with linear and nonlinear viscous dampers. *J Constr Steel Res*. 2018;148:409–21.
16. Pavlou E, Constantinou MC. Response of nonstructural components in structures with damping systems. *J Struc Eng*. 2006;132(7):1108–17.
17. Lavan O, Dargush GF. Multi-objective evolutionary seismic design with passive energy dissipation systems. *J Earthq Eng*. 2009;13(6):758–90.
18. Raheem SEA. Mitigation measures for earthquake induced pounding effects on seismic performance of adjacent buildings. *Bull Earthq Eng*. 2014;12(4):1705–24.
19. Raheem SEA, Fooly MY, Omar M, Zaher AKA. Seismic pounding effects on the adjacent symmetric buildings with eccentric alignment. *Earthq Struct*. 2019;16(6):715–26.
20. Rezavandi A, Moghadam AS. Experimental and numerical study on pounding effects and mitigation techniques for adjacent structures. *Adv Struct Eng*. 2007;10(2):121–34.
21. Lasowicz N, Kwiecień A, Jankowski R. Experimental study on the effectiveness of polymer damper in damage reduction of temporary steel grandstand. *J Phys Conf Ser*. 2015;628(1):012051.
22. Stręk AM, Lasowicz N, Kwiecień A, Zając B, Jankowski R. Highly dissipative materials for damage protection against earthquake-induced structural pounding. *Materials*. 2021;14(12):3231.
23. Polycarpou PC, Komodromos P, Polycarpou AC. A nonlinear impact model for simulating the use of rubber shock absorbers for mitigating the effects of structural pounding during earthquakes. *Earthq Eng Struct Dyn*. 2013;42(1):81–100.
24. Takabatake H, Yasui M, Nakagawa Y, Kishida A. Relaxation method for pounding action between adjacent buildings at expansion joint. *Earthq Eng Struct Dyn*. 2014;43(9):1381–400.
25. Jankowski R, Mahmoud S. Linking of adjacent three-storey buildings for mitigation of structural pounding during earthquakes. *Bull Earthq Eng*. 2016;14(11):3075–97.
26. Patel CC, Jangid RS. Seismic response of dynamically similar adjacent structures connected with viscous dampers. *IES J Part A Civ Struct Eng*. 2010;3(1):1–13.
27. Pratesi F, Sorace S, Terenzi G. Seismic pounding mitigation of a modern heritage R/C bell tower. *WIT Trans Built Environ*. 2013;131:303–14.
28. Sorace S, Terenzi G. Damped interconnection-based mitigation of seismic pounding between adjacent R/C buildings. *Int J Eng Technol*. 2013;5(3):406.
29. Pratesi F, Sorace S, Terenzi G. Analysis and mitigation of seismic pounding of a slender R/C bell tower. *Eng Struct*. 2014;71:23–34.
30. Kandemir-Mazanoglu EC, Mazanoglu K. An optimization study for viscous dampers between adjacent buildings. *Mech Syst Signal Process*. 2017;89:88–96.
31. Kazemi F, Mohebi B, Yakhchalian M. Enhancing the seismic performance of adjacent pounding structures using viscous dampers. In: *The 16th European conference on earthquake engineering (16ECEE)*; 2018, pp. 18–21.
32. Bekdaş G, Nigdeli SM. Preventing the pounding of adjacent buildings with harmony search optimized tuned mass damper. In: *3rd European conference of civil engineering*; 2012, pp. 2–4.
33. Licari M, Sorace S, Terenzi G. Nonlinear modeling and mitigation of seismic pounding between R/C frame buildings. *J Earthq Eng*. 2015;19(3):431–60.
34. Tubaldi E, Barbato M, Ghazizadeh S. A probabilistic performance-based risk assessment approach for seismic pounding with efficient application to linear systems. *Struct Saf*. 2012;36:14–22.
35. Martinez-Rodrigo M, Romero ML. An optimum retrofit strategy for moment resisting frames with nonlinear viscous dampers for seismic applications. *Eng Struct*. 2003;25(7):913–25.
36. Bigdeli K, Hare W, Tesfamariam S. Configuration optimization of dampers for adjacent buildings under seismic excitations. *Eng Optim*. 2012;44(12):1491–509.
37. Dall'Asta A, Tubaldi E, Ragni L. Influence of the nonlinear behavior of viscous dampers on the seismic demand hazard of building frames. *Earthq Eng Struct Dyn*. 2015;45(1):149–69.
38. Mansoori MR, Moghadam AS. Using viscous damper distribution to reduce multiple seismic responses of asymmetric structures. *J Constr Steel Res*. 2009;65(12):2176–85.
39. Kazemi F, Miari M, Jankowski R. Investigating the effects of structural pounding on the seismic performance of adjacent RC and steel MRFs. *Bull Earthq Eng*. 2021;19(1):317–43.
40. ASCE 7-16. Minimum design loads and associated criteria for buildings and other structures. Reston, VA: American Society of Civil Engineers; 2017.
41. AISC Committee. Specification for structural steel buildings (ANSI/AISC 360-16). Chicago-Illinois: American Institute of Steel Construction; 2016.
42. AISC A. AISC 341-16, seismic provisions for structural steel buildings. Chicago, IL: American Institute of Steel Construction; 2016.
43. ACI Committee, International Organization for Standardization. Building code requirements for structural concrete (ACI 318-14) and commentary. American Concrete Institute; 2014.
44. Kitayama S, Constantinou MC. Seismic performance of buildings with viscous damping systems designed by the procedures of ASCE/SEI 7-16. *J Struct Eng*. 2018;144(6):04018050.
45. Haselton CB. Assessing seismic collapse safety of modern reinforced concrete moment frame buildings. Doctoral dissertation, Stanford University; 2006.
46. Kazemi F, Mohebi B, Jankowski R. Predicting the seismic collapse capacity of adjacent SMRFs retrofitted with fluid viscous

- dampers in pounding condition. *Mech Syst Signal Process.* 2021;161: 107939.
47. Lignos DG, Krawinkler H. Deterioration modeling of steel components in support of collapse prediction of steel moment frames under earthquake loading. *J Struct Eng.* 2010;137(11):1291–302.
 48. Ibarra LF, Medina RA, Krawinkler H. Hysteretic models that incorporate strength and stiffness deterioration. *Earthq Eng Struct Dyn.* 2005;34(12):1489–511.
 49. McKenna F, Fenves GL, Filippou FC, Scott MH. Open system for earthquake engineering simulation (OpenSees). Berkeley: Pacific Earthquake Engineering Research Center, University of California; 2016.
 50. Altoontash A. Simulation and damage models for performance assessment of reinforced concrete beam–column joints. Doctoral dissertation, Stanford University; 2004.
 51. Fardis MN, Biskinis DE. Deformation capacity of RC members, as controlled by flexure or shear. In: Otani symposium, vol. 511530; 2003.
 52. Berry M, Parrish M, Eberhard M. PEER structural performance database user's manual. Berkeley: University of California; 2004.
 53. Deierlein GG, Haselton CB. Benchmarking the collapse safety of code-compliant reinforced concrete moment frame building systems. In: ATC/JSCA US-Japan workshop on improvement of structural design and construction practices, proceedings of an international workshop; 2005, pp. 17–9.
 54. Mohebi B, Yazdanpanah O, Kazemi F, Formisano A. Seismic damage diagnosis in adjacent steel and RC MRFs considering pounding effects through improved wavelet-based damage-sensitive feature. *J Build Eng.* 2021;33:101847.
 55. Mahmoud S, Jankowski R. Modified linear viscoelastic model of earthquake-induced structural pounding. *Iran J Sci Technol Trans Civ Eng.* 2011;35(C1):51–62.
 56. Yazdanpanah O, Mohebi B, Kazemi F, Mansouri I, Jankowski R. Development of fragility curves in adjacent steel moment-resisting frames considering pounding effects through improved wavelet-based refined damage-sensitive feature. *Mech Syst Signal Process.* 2022;173: 109038.
 57. Anagnostopoulos SA. Equivalent viscous damping for modeling inelastic impacts in earthquake pounding problems. *Earthq Eng Struct Dyn.* 2004;33(8):897–902.
 58. Mahmoud S, Jankowski R. Elastic and inelastic multi-storey buildings under earthquake excitation with the effect of pounding. *J Appl Sci.* 2009;9(18):3250–62.
 59. Polycarpou PC, Komodromos P. Earthquake-induced poundings of a seismically isolated building with adjacent structures. *Eng Struct.* 2010;32(7):1937–51.
 60. Karayannis CG, Naoum MC. Torsional behavior of multistory RC frame structures due to asymmetric seismic interaction. *Eng Struct.* 2018;163:93–111.
 61. Applied Technology Council, United States. Federal Emergency Management Agency. Quantification of building seismic performance factors. US Department of Homeland Security, FEMA; 2009.
 62. Asgarkhani N, Yakhchalian M, Mohebi B. Evaluation of approximate methods for estimating residual drift demands in BRBFs. *Eng Struct.* 2020;224: 110849.
 63. Kazemi F, Jankowski R. Enhancing seismic performance of rigid and semi-rigid connections equipped with SMA bolts incorporating nonlinear soil–structure interaction. *Eng Struct.* 2022;114896.
 64. Kazemi F, Jankowski R. Machine learning-based prediction of seismic limit-state capacity of steel moment-resisting frames considering soil–structure interaction. *Comput Struct.* 2022. <https://doi.org/10.1016/j.compstruc.2022.106886>.
 65. MATLAB. Simulink as a Technical Computing Language. Engineering Computations and Modeling in MATLAB; 2018.
 66. FEMA-356. Prestandard and commentary for the seismic rehabilitation of buildings. Washington, DC: Federal Emergency Management Agency; 2000.

Publisher's Note Springer Nature remains neutral with regard to jurisdictional claims in published maps and institutional affiliations.